

Heteronuclear Parahydrogen-Induced Hyperpolarization via Side Arm Hydrogenation

Oleg G. Salnikov,^{*,[a]} Nikita V. Chukanov,^[a] Andrey N. Pravdivtsev,^[b] Dudari B. Burueva,^[a] Sergey V. Sviyazov,^[a,c] Jan-Bernd Hövener,^[b] and Igor V. Koptug^[a]

[a] Dr. O. G. Salnikov, Dr. N. V. Chukanov, Dr. D. B. Burueva, S. V. Sviyazov, Prof. I. V. Koptug
Laboratory of Magnetic Resonance Microimaging
International Tomography Center SB RAS
3A Institutskaya St., Novosibirsk 630090, Russia
E-mail: salnikov@tomo.nsc.ru

[b] Dr. A. N. Pravdivtsev, Prof. J.-B. Hövener
Section Biomedical Imaging, Molecular Imaging North Competence Center (MOIN CC), Department of Radiology and Neuroradiology
University Medical Center Schleswig-Holstein and Kiel University
24118 Kiel, Germany

[c] S. V. Sviyazov
Novosibirsk State University
2 Pirogova St., Novosibirsk 630090, Russia

Abstract: Nuclear spin hyperpolarization dramatically enhances the sensitivity of nuclear magnetic resonance spectroscopy and imaging. Hyperpolarization of biomolecules (e.g., pyruvate) is of particular interest as it allows one to follow their metabolism, providing a diagnostic tool for various pathologies, including cancer. In this regard, the hyperpolarization of ^{13}C nuclei is especially beneficial due to its relatively long hyperpolarization lifetime and the absence of a background signal. Parahydrogen-induced polarization (PHIP) is arguably the most affordable hyperpolarization technique. PHIP exploits the pairwise addition of parahydrogen to an unsaturated substrate. This sets limitations on the range of compounds amenable to direct PHIP hyperpolarization. The range of molecules that can be hyperpolarized with PHIP significantly expanded in 2015 when PHIP by means of side arm hydrogenation (PHIP-SAH) was introduced. Here, parahydrogen is added to an unsaturated alcoholic moiety of an ester followed by polarization transfer to carboxylate ^{13}C nuclei with a subsequent cleavage of the side arm. In this review, the recent advances in PHIP-SAH are discussed, including the synthetic methodology to produce isotopically labeled precursors, peculiarities of pairwise addition of parahydrogen to PHIP-SAH precursors, polarization transfer, cleavage of the side arm, purification of hyperpolarized solution, and, finally, in vitro and in vivo applications.

1. Introduction

Nuclear magnetic resonance (NMR) spectroscopy and magnetic resonance imaging (MRI) are used in various applications in chemistry, biology, and medicine. However, these techniques have intrinsically low sensitivity originating from low differences in populations of nuclear spin energy levels even at high magnetic fields of modern NMR spectrometers. For example, at 9.4 T and 298 K only one ^1H nucleus out of ca. 31000 contributes to an observed NMR signal. Hence, there is a hidden potential for a drastic improvement in NMR sensitivity. Therefore, hyperpolarization techniques, which dramatically enhance nuclear spin polarization (P) by up to several orders of magnitude, have rapidly developed in recent years.^[1–5] These techniques have many established and prospective applications, for example, production of hyperpolarized (HP) molecular contrast agents for magnetic resonance spectroscopy (MRS) and imaging reporting on aberrant metabolism in tissues,^[4,6,7] production of HP gases for lung MRI,^[8–10] metabolomics,^[3,11] structural biology,^[5,12,13] mechanistic studies of chemical transformations,^[14–18] materials science,^[19–21] batteries research,^[22] etc. HP state relaxes to thermal equilibrium with a rate typically characterized

by spin-lattice relaxation time (T_1) of corresponding spins. As a result, for solution-state applications, it is generally preferable to hyperpolarize spin- $\frac{1}{2}$ heteronuclei, e.g. ^{13}C ^[7,23] or ^{15}N ,^[24] which typically have several times greater T_1 in solution compared to protons. In addition, the natural abundance of ^{13}C and ^{15}N is low; hence, without hyperpolarization and isotopic labeling, observed spectra essentially have no background.

The most common solution-state hyperpolarization techniques are dissolution dynamic nuclear polarization (dDNP),^[25–27] parahydrogen-induced polarization (PHIP),^[28,29] and signal amplification by reversible exchange (SABRE).^[30,31] dDNP employs high thermal polarization of electron spins in radicals at high magnetic fields and cryogenic temperatures as a source of nuclear hyperpolarization.^[26] Under microwave irradiation, electron polarization is transferred to the nearby nuclear spins. Next, the sample is rapidly dissolved in hot water, giving an aqueous solution of an HP compound of interest. The most common HP tracer in a number of pre-clinical and clinical studies^[32–34] is [$1\text{-}^{13}\text{C}$]pyruvate polarized with dDNP. Upon administration, pyruvate undergoes rapid metabolic transformations predominantly to lactate, alanine, and bicarbonate. Following the rates of these processes allows for identifying abnormalities in metabolism that could be

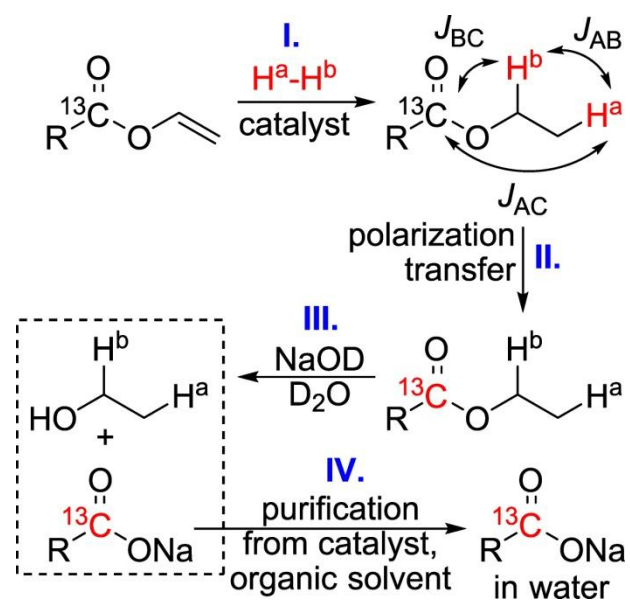
associated with a cancerous tumor.^[35] However, this technology is still available only at selected sites worldwide because it requires expensive and complicated equipment. Moreover, common dDNP protocol which uses direct polarization of ¹³C spins is relatively low-throughput, as preparation of a highly polarized sample takes ~1 hour.

PHIP and SABRE use parahydrogen (p-H₂, singlet-state nuclear spin isomer of H₂) as a source of non-equilibrium spin order. In PHIP, p-H₂ is added to a double or a triple bond in an unsaturated substrate. The key requirement is that the two atoms from the same p-H₂ molecule should end up in the same molecule of reaction product (pairwise addition).^[36] If these two H atoms retain spin correlation between them and end up in magnetically inequivalent positions, observable hyperpolarization is created. If the addition of p-H₂ occurs at a high magnetic field (at which the chemical shift difference is much larger than mutual scalar spin-spin interaction), so-called PASADENA^[28] (parahydrogen and synthesis allow dramatically enhanced nuclear alignment) experiment, multiplet polarization of the nascent p-H₂ protons is obtained. In the case of pairwise addition at a low magnetic field followed by adiabatic transfer to a high field, i.e. ALTADENA^[37] (adiabatic longitudinal transport after dissociation engenders net alignment) experiment, net polarization of each proton is produced, which could be also distributed across other protons in the *J*-coupled network. In SABRE, p-H₂ and to-be-hyperpolarized substrate reversibly bind to a metal complex. Polarization transfer within the complex (either spontaneous at a low magnetic field, or driven by radiofrequency (RF) irradiation) enables hyperpolarization of the substrate.^[38–40] Hence, PHIP and SABRE hyperpolarization require only a substrate, a catalyst, and parahydrogen. The cryogens are necessary only for the preparation of parahydrogen, which, once prepared, can be stored over weeks and used on demand.^[41] Therefore, PHIP and SABRE are significantly more accessible than dDNP.

Since PHIP requires pairwise hydrogen addition, the range of compounds which can be directly polarized using this approach is relatively limited to those having corresponding unsaturated precursors. Therefore, 2-hydroxyethyl propionate (HEP), succinate and their derivatives were the most commonly hyperpolarized tracers for a long time.^[42–44] However, such biologically important carboxylate metabolites as pyruvate and acetate were inaccessible. The straightforward approach was to introduce an unsaturated side chain that can be hydrogenated with p-H₂; this method received the name PHIP-label and enabled hyperpolarization of amino acids and peptides.^[45–47] However, the resulting hyperpolarized tracers were not in their native state, and their biological relevance was not obvious.

An elegant extension of this approach proposed in 2015 by Reineri et al.^[48] provided a strategy to overcome this issue (Scheme 1). Here, an ester with an unsaturated alcoholic moiety is employed as a PHIP precursor. After hyperpolarization, the hydrogenated moiety (also referred to as a side arm) could be cleaved, and the resulting HP tracer could be extracted into the aqueous phase. This PHIP by means of side arm hydrogenation (PHIP-SAH)

method enabled hyperpolarization of previously inaccessible compounds in their native forms.^[48] Since its discovery, the technique has been rapidly developing toward clinical applications, with several preclinical trials demonstrated.^[49–51] Here, we will be reviewing the progress in all aspects of PHIP-SAH, including synthesis of isotopically labeled precursors, optimization of their structure with respect to the resultant polarization efficiency, novel low-field and high-field polarization transfer schemes, optimization of HP substrate purification protocols, and, finally, promising applications in vitro and in vivo.



Scheme 1. Schematics of PHIP-SAH process on the example of vinyl ester precursor. Step I: Catalytic pairwise addition of p-H₂ (denoted here as H^a-H^b to emphasize the protons that originated from p-H₂) to an unsaturated ester precursor. Step II: Polarization transfer from nascent H^a and H^b protons to carboxylic ¹³C nucleus mediated by the *J*-coupling network. Step III: Cleavage of the ester group via alkaline hydrolysis. Step IV: purification of HP carboxylate from catalyst and organic solvent to produce an aqueous solution of ¹³C-HP carboxylate.

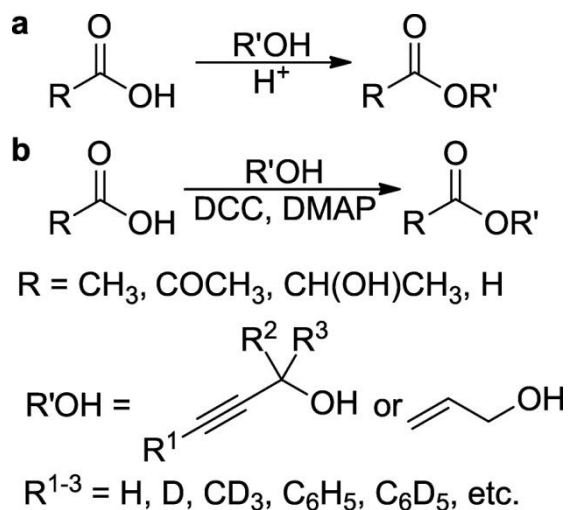
2. Synthesis of unsaturated precursors for PHIP-SAH

To perform PHIP-SAH, one must first synthesize a corresponding unsaturated precursor for the target HP tracer. The PHIP-SAH precursor consists of the target tracer, typically ¹³C labeled to increase the resulting molar polarization payload, and the unsaturated moiety (side arm). Depending on the polarization transfer strategies employed, the side arm can also be selectively ²H/¹³C or ²H uniformly labeled.

The most popular carboxylates (targets) which were employed in PHIP-SAH are pyruvate and acetate, which is not unexpected considering their important metabolic roles^[52,53] (although PHIP-SAH polarization of other carboxylates was also reported^[54–56]). The typical unsaturated side arms are vinyl, propargyl, and various substituted propargyl-based moieties.^[57,58]

The synthesis of propargyl, substituted propargyl,

and allyl ester precursors for PHIP-SAH is relatively straightforward and typically exploits either an acid-catalyzed esterification^[57,59] or a coupling of an alcohol and a carboxylic acid mediated by *N,N'*-dicyclohexylcarbodiimide (DCC)^[58,59] (Scheme 2).

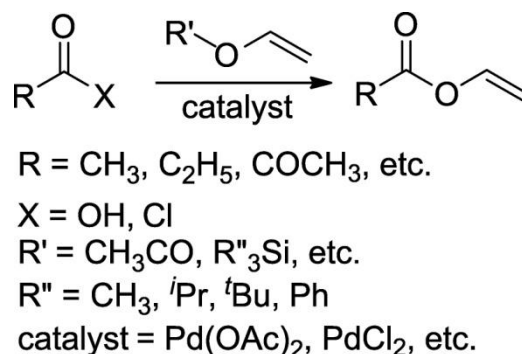


Scheme 2. General approaches for the synthesis of propargyl, substituted propargyl or allyl ester precursors for PHIP-SAH via (a) acid-catalyzed esterification or (b) DCC-mediated coupling.

Of particular interest is the synthesis of isotopically labeled and substituted propargyl side arms, which allows for the increase of polarization transfer efficiency. Glöggl and co-workers made substantial efforts in this regard, developing syntheses of various isotopologues of 3-phenylprop-2-ynyl pyruvate tailored for the efficient performance of high field polarization transfer schemes.^[58,60,61] In particular, a ¹³CD₂ group was introduced in position 1 of the alcoholic moiety via Favorskii reaction of phenylacetylene and

[¹³C]formaldehyde-d₂.^[60,61] The corresponding product of pairwise p-H₂ addition, HP *cis*-[1-¹³C]cinnamyl-1,1-d₂ [1-¹³C]pyruvate, represents an example of a system with an efficient polarization transfer demonstrating *P*_{13C} of up to 25%. The same group also explored hyperpolarization of pyruvate and acetate using [2-¹³C]-3-phenylprop-2-ynyl-1,1-d₂ moiety.^[58,62] For this, the synthesis of [1-¹³C]phenylacetylene was accomplished in 5 steps starting from ¹³CD₃I and benzaldehyde.^[58]

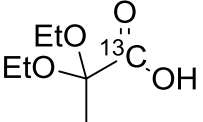
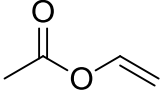
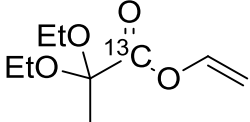
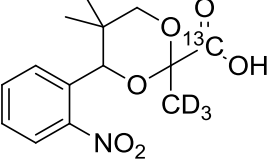
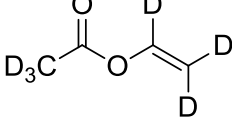
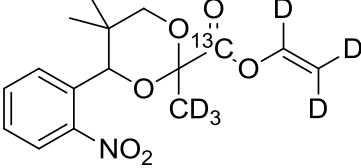
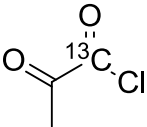
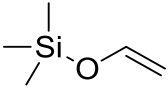
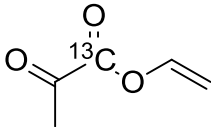
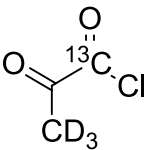
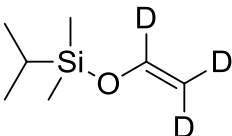
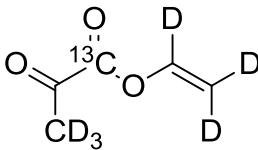
The synthesis of vinyl esters appears to be more challenging, since it cannot be accomplished by simple esterification. The most obvious method involves transvinylation reaction between the acid of interest with a significant excess of a vinyl ester of another carboxylic acid in the presence of a metal catalyst (Scheme 3).^[63,64] The catalyst is usually a ruthenium or a palladium salt with the addition of sodium salt of the acid of interest or a base. The transvinylation reaction is suitable if the product can be easily isolated from the reaction mixture, for example, by distillation. A number of vinyl ester precursors for PHIP-SAH have been synthesized following this approach (Table 1).^[54,57,65-69]



Scheme 3. General approach for the synthesis of vinyl ester precursors for PHIP-SAH via transvinylation.

Table 1. The summary of the published syntheses of vinyl carboxylate precursors for PHIP-SAH using transvinylation approach.

Substrate	Reagent	Catalyst	Product	Yield, %	Ref.
		RuCl ₃ 5 mol% CH ₃ ¹³ CO ₂ Na 6.5 mol%		98	[65]
		Pd(OAc) ₂ 0.5 mol% KOH 10.5 mol%		7[a]	[66]
		Pd(OAc) ₂ 1 mol% KOH 10 mol%		15	[54]
		Pd(OAc) ₂ 20 mol% KOH 13 mol%		6	[57]

		Pd(OAc) ₂ Py ₂ 0.5 mol%		19	[67]
		Pd(OAc) ₂ 1 mol% KOH 10 mol%		81	[68]
		PdCl ₂ 4 mol%		67	[69]
		PdCl ₂ 4 mol%		45	[69]

^aYield is not reported.

For regular aliphatic acids (e.g., acetic,^[65] propionic,^[66] and lactic acids^[54]), ruthenium chloride and palladium acetate are well suited as a transvinylation catalytic system. However, this approach was inefficient for synthesizing vinyl pyruvate, providing only 6% yield.^[57] Carrera et al. proposed to protect the carbonyl group of pyruvic acid by forming a diethyl ketal.^[67] This increased the yield of the transvinylation step to 19%, although the total yield of the vinyl pyruvate product over three steps was only ca. 8%.^[67] Ding et al. developed this approach further by using a photolabile protecting group, which boosted the yield at the transvinylation step to 81%.^[68] However, the overall yield over the four steps was only 3%, primarily due to the low efficiency of the deprotection step. The most significant advance in the synthesis of vinyl pyruvate was achieved by Brahms et al.^[69] Their approach is based on performing transvinylation reaction between pyruvoyl chloride and a vinyloxy silane catalyzed by PdCl₂. The obtained yields of transvinylation step were boosted up to 67%. Later, the same group refined and adopted this approach to other vinyl α -ketocarboxylates, particularly vinyl 2-oxobutyrates, divinyl α -ketoglutarate, divinyl oxaloacetate.^[55] For efficient polarization transfer at high magnetic fields, deuteration of vinyl side arm is preferable. To achieve this, Brahms et al. also developed a two-step synthesis of vinyloxy silanes-d₃ starting from THF-d₈.^[55,69]

3. Pairwise parahydrogen addition to side arm

The first step of the PHIP-SAH process is the pairwise addition of p-H₂ to an unsaturated side arm, which is typically catalyzed by a cationic rhodium complex,^[70] although heterogeneous supported metal catalysts can also be used,^[16,71] this approach is detailed in Section 5. To maximize an attainable heteronuclear NMR signal of an HP reaction product, one needs to first maximize

molar ¹H polarization (i.e., product of P_{1H} level (%) and concentration). Both are affected by various factors such as the substrate structure (side arm and carboxylic moiety), catalyst, solvent, concentrations, hydrogen pressure, and temperature.

Salnikov et al. systematically investigated the efficiency of PHIP-SAH of acetate and pyruvate esters with ethyl, propyl, and allyl side arms using corresponding vinyl, allyl, and propargyl precursors and methanol-d₄ as the solvent.^[72] The highest ¹H polarizations (P_{1H}) were obtained for ethyl acetate (8.1%) and allyl pyruvate (21%), while propyl esters were found to be the least efficient. The measured pseudo-first order rate constants for hydrogenation of propargyl esters were found to be approximately an order of magnitude greater than those of vinyl and allyl esters. Reineri and co-workers confirmed these trends for lactate and pyruvate esters—the use of propargyl precursors resulted in ca. 2–2.5 times higher P_{1H} compared to the case of vinyl substrates.^[54,67]

The effect of the carboxylic moiety structure was not studied in much detail. This is understandable, considering that the choice of carboxylate is primarily motivated by its prospective biomedical applications. However, recently, Brahms et al. investigated PHIP-SAH polarization of several ethyl carboxylates and found that «regular» vinyl esters (namely, vinyl acetate and vinyl octanoate) are hydrogenated considerably faster than electron-poor vinyl pyruvate and vinyl 2-oxobutyrates.^[55] Moreover, in the hydrogenation of divinyl α -ketoglutarate the two vinyl groups differ in reactivity following these trends. The same team also explored the feasibility of producing HP carboxylates using trivinyl orthoester precursors, namely trivinyl orthoacetate.^[73] However, this approach was found to be inefficient as hydrogenation of trivinyl orthoacetate led to the formation of many side products.

Typically, PHIP-SAH studies employ cationic Rh complexes with bidentate phosphine ligands, e.g.,

$[\text{Rh}(\text{COD})(\text{dppb})]^+$ or $[\text{Rh}(\text{NBD})(\text{dppb})]^+$ ($\text{dppb} = 1,4$ -bis(diphenylphosphino)butane), as hydrogenation catalysts, which is understandable as they are commercially available. However, Itoda et al. showed that the use of bidentate phosphines with PCy_2 groups provides significantly higher conversion levels of vinyl acetate and propargyl acetate compared to the standard dppb -catalyst (Figure 1) as a result of a ca. 2-fold increase in turnover frequency (TOF) and a ca. 4-fold increase in the catalyst activation rate.^[74] The resulting polarization levels were slightly improved as well.

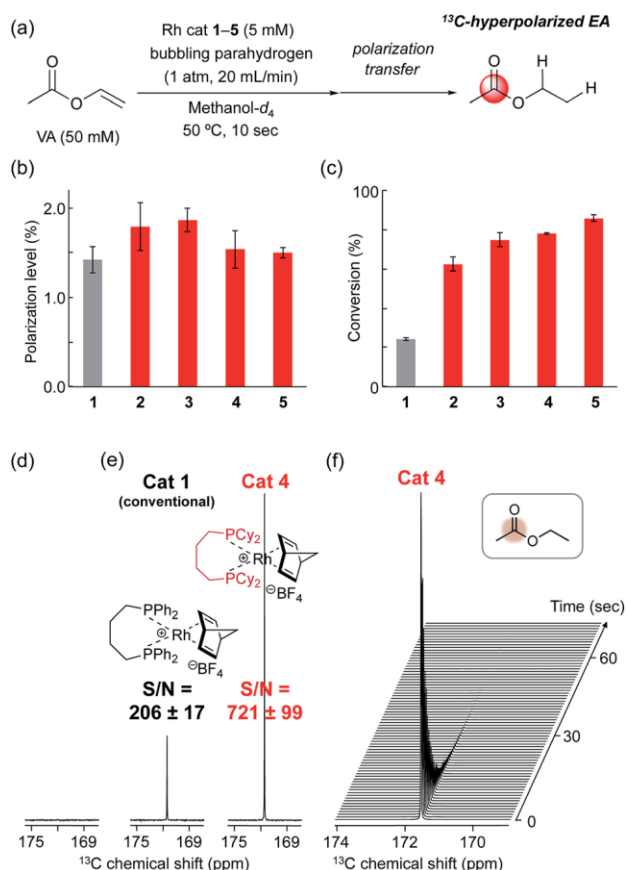


Figure 1. (a) Scheme of ¹³C PHIP-SAH of ethyl acetate (EA) using vinyl acetate (VA) precursor. (b) ¹³C polarization levels of EA and (c) conversion rates of VA using catalyst precursors 1–5. (d) ¹³C NMR spectrum of naturally abundant ¹³C EA (ca. 40 mM) at thermal equilibrium. (e) ¹³C NMR spectra of HP EA produced using catalysts 1 or 4 (initial concentration of VA 50 mM). S/N is a signal-to-noise ratio. (f) Stacked ¹³C NMR spectra of relaxing HP EA. **1** = $[\text{Rh}(\text{NBD})(\text{dppb})]\text{BF}_4$, **2** = $[\text{Rh}(\text{NBD})(\text{dcpe})]\text{BF}_4$, **3** = $[\text{Rh}(\text{NBD})(\text{dcpp})]\text{BF}_4$, **4** = $[\text{Rh}(\text{NBD})(\text{dcpb})]\text{BF}_4$, **5** = $[\text{Rh}(\text{NBD})(\text{dcpf})]\text{BF}_4$. Adapted from Ref. ^[74] published under a permissive Creative Commons Attribution 3.0 Unported License (CC BY-NC 3.0) by the Royal Society of Chemistry.

The solvent nature is an important factor in PHIP-SAH process, affecting both hydrogenation and hyperpolarization efficiency. Bondar et al. systematically investigated solvent effects in the hyperpolarization of $[1\text{-}^{13}\text{C}]\text{pyruvate}$ using the corresponding propargyl precursor.^[75] Acetone-d₆ demonstrated a ca. 2 times higher TOF than other solvents tested (methanol-d₄, toluene, 95:5 v/v toluene/ethanol mixture, CDCl_3 , and

95:5 v/v $\text{CDCl}_3/\text{ethanol}$ mixture), apparently as a result of a higher lability of acetone ligand in the Rh complex coordination sphere compared to methanol and substrate (the latter inevitably fills the vacant sites when non-coordinating toluene or chloroform solvents are used). However, the highest polarization levels ($P_{1\text{H}} = 21\%$, $P_{13\text{C}} = 9.2\%$) were obtained in methanol-d₄, likely as a result of the lowest contribution of singlet/triplet mixing in intermediate complexes in the catalytic cycle.^[76,77] Aqueous-phase PHIP-SAH using a water-soluble cationic Rh complex was also explored in some studies.^[67,72] However, one should note that biomedical applications of PHIP-SAH require the separation of HP carboxylate from the catalyst and the solvent, making it impractical to use such solvents as alcohols and water (see Section 5 for details). Moreover, vinyl esters are not compatible even with such solvents as acetone, as traces of water induce cleavage of the side arm before hydrogenation.^[78,79]

The effect of concentrations on PHIP-SAH efficiency can be viewed as a double-edged sword. One can use extremely low sub-millimolar substrate concentrations (even having the catalyst in excess with respect to the substrate), and obtain impressive ¹H and ¹³C polarization levels on the order of 50–60%.^[80] However, the prospective biomedical applications require high molar polarization, so a balance should be found. At the same time, high substrate concentrations result in a dramatic decrease in polarization levels due to detrimental interactions of the high magnetization of the sample with the NMR resonator, described in detail below in Section 4.6.

There are other sources of polarization losses directly related to the peculiarities of the hydrogenation step. A slow rate of hydrogenation can lead to increased detrimental effects of nuclear spin relaxation in the product and reaction intermediates during hydrogenation^[81] and S-T₀ conversion.^[82–84] Another factor is the possibility of non-pairwise p-H₂ addition, which is especially relevant for heterogeneous catalysts.^[16,85] The typical approaches to circumvent these polarization losses are to accelerate the reaction by heating the hydrogenation reactor,^[79] increasing p-H₂ pressure and flow,^[79,81] or using vigorous shaking,^[48] and rational choice of hydrogenation catalyst.^[74]

4. Polarization transfer to heteronuclei

The efficiency of polarization transfer from the added p-H₂ to the heteronucleus in PHIP-SAH experiments essentially depends on the starting point and the evolution and manipulations thereafter—both points are discussed in the following sub-sections in the context of polarization transfer.

4.1. Initial spin order

The product acquires a nuclear spin order of p-H₂ upon hydrogenation, initially at a singlet state. The spin order survives the chemical addition, an essential requirement for all subsequent steps. When the two protons stemming from p-H₂ are strongly coupled, e.g., at low magnetic fields under the so-called ALTADENA conditions,^[37] the singlet state of the two spins is an eigenstate of the

system. Hence, in the product the singlet spin state described with the following density matrix is populated:

$$\hat{\rho}_S = |S\rangle\langle S| = \frac{\hat{1}}{4} - (\hat{I}_x^a \hat{I}_x^b + \hat{I}_y^a \hat{I}_y^b + \hat{I}_z^a \hat{I}_z^b) \quad (\text{Eq. 1})$$

where a and b are nuclei spin designators (see Figure 2a), x, y, z are Cartesian axes, $\hat{1}$ is a unitary operator and \hat{I}_x^a, \hat{I}_y^a etc. are the corresponding nuclear spin operators. Here, it is assumed that pure p-H₂ (i.e., 100% p-H₂ enrichment) was used and relaxation is negligible. The same spin order can be achieved even at a high magnetic field if a sufficiently strong continuous wave (CW) irradiation or a decoupling RF pulse is applied.^[82,86,87]

When the experiment is carried out in the weak coupling regime instead, e.g., at a high magnetic field under the so-called PASADENA conditions,^[28] the singlet spin state is not an eigenstate of the system of these two chemically inequivalent spins. As the HP product formation events are distributed over time, when the spin order of p-H₂ is projected on a new spin system, only one element of the singlet spin state (the one parallel to an external magnetic field) is preserved, given by the following density matrix:

$$\hat{\rho} = \frac{\hat{1}}{4} - \hat{I}_z^a \hat{I}_z^b \quad (\text{Eq. 2})$$

(again, assuming pure p-H₂ and neglecting relaxation).

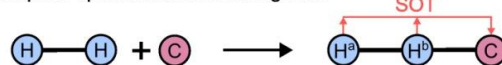
In reality, additional interactions in the product and catalyst perturb the spin state of nascent protons.^[82] For a more detailed analysis of these factors, we refer the reader to the insightful review by Natterer and Bargon.^[88] At the same time, these interactions enable spin order transfer to other nuclei.

4.2. An ideal spin system

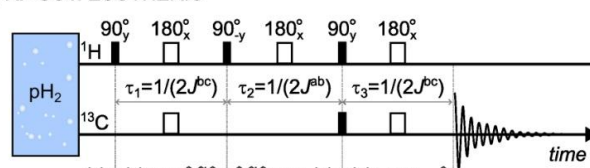
The typical spin system of PHIP-SAH tracer is characterized by two vicinal protons on the side arm (originating from p-H₂), a target ¹³C nucleus of the carboxylic moiety 3–5 bonds away from them, and other protons, deuterons, or ¹³C nuclei, depending on the chosen molecule (a simplified scheme is presented in Figure 2a). While the J couplings between the p-H₂-derived protons, J^{ab} , are usually relatively strong, on the order of 7–11 Hz, the couplings to the ¹³C, J^{ac} and J^{bc} , are typically weaker^[89] (here a and b denote the two nascent p-H₂ protons, with the latter one being closer to the ¹³C nucleus than the former; c denotes ¹³C nucleus, see Figure 2). For example, for ethyl pyruvate, $J^{ab} = 7.1$ Hz, $J^{bc} = 3$ Hz and $J^{ac} \approx -0.1$ Hz.^[90] In contrast, in allyl pyruvate the heteronuclear J couplings of interest are much weaker, $J^{bc} = -0.18$ Hz and $J^{ac} = 0.2$ Hz.^[91] Thus, vinyl esters are considered to be the most attractive precursors for PHIP-SAH due to stronger interactions enabling much faster direct polarization transfer. The duration of the polarization transfer is critical due to the effects of relaxation.

At the same time, the allyl ester motif turned out to be also very efficient in polarizing distant ¹³C nuclei despite almost negligible direct couplings between the nascent ¹H and target ¹³C nuclei. For this, an additional ¹H or ¹³C spin is introduced in-between; the polarization is transferred from the added HP protons to the target ¹³C via this intermediate nucleus (e.g., ¹³C as a part of ¹³CD₂^[60,62] or ¹H as a part of CDH^[92]) as discussed below.

a) Graph of spin interactions during PHIP



b) RF-SOT: ESOTHERIC



c) Magnetic field cycling

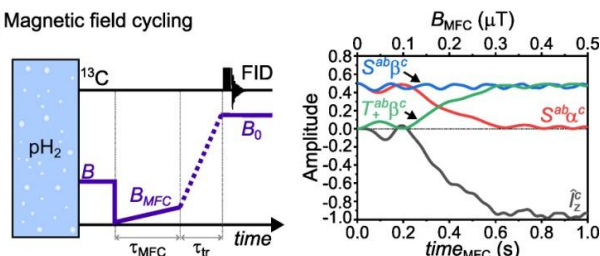


Figure 2. Schematic of spin order transfer in PHIP-SAH experiments. (a) A simplistic H^aH^bC PHIP-SAH spin system, e.g., a simplification of ethyl pyruvate where only two p-H₂-derived protons and ¹³C carboxyl nucleus are considered, and spin-spin interaction J^{ac} is set to zero (in reality it is a small but nonzero value, ca. -0.1 Hz), two other interactions are $J^{bc} = 3$ Hz and $J^{ab} = 7.1$ Hz. (b) For this system, ESOTHERIC RF-SOT allows for complete polarization transfer from $\hat{I}_z^a \hat{I}_z^b$ to \hat{I}_z^c . Note that the spin order diagram here ignores coefficients for simplicity. (c) For this system, MFC with a simple linear ramp of the magnetic field, $B_{MFC}(time_{MFC})$, from 0 to 0.5 μ T during 1 s also enables the complete transfer of population from $S^{ab}\alpha^c$ state to $T^+_{ab}\beta^c$, while $S^{ab}\beta^c$ retains its population. Hence, starting with equal populations of α^c and β^c states (no polarization on ¹³C), in the end, MFC results in 100% population of the β^c state or maximum (here negative) net polarization of ¹³C $-\hat{I}_z^c$. Here, the dashed line in the magnetic field profile indicates that the field will eventually increase, but during the sample transfer, this field is less critical for SOT and typically not well controlled.

Deuterating a PHIP-SAH precursor simplifies the spin system, making the polarization transfer more efficient due to the symmetry of spin-spin interactions. For example, it is impossible to hyperpolarize the carboxyl ¹³C nucleus of ethyl esters to more than 50%.^[93] However, deuteration resolves this restriction by breaking the symmetry constraints and making the spin system at high field essentially an AMX system with up to 100% polarization transfer allowed theoretically.

4.3. Polarization via RF irradiation in a weak coupling regime (at high magnetic fields)

Many RF pulse sequences for polarization transfer are ascending back to the insensitive nuclei enhanced by polarization transfer (INEPT) pulse sequence developed by Morris and Freeman in 1979.^[94] In a very detailed and complete review at the time, Green et al. in 2012 described the physics of INEPT and its modifications for p-H₂-related experiments.^[95]

The parahydrogen and INEPT-enabled hyperpolarization (phINEPT+) sequence was one of the

first high-field RF pulse sequences developed for the transfer of PHIP to heteronuclei.^[96] Here, “+” traditionally stands for the refocused version of INEPT, where in-phase polarization on heteronuclei is generated, and the first pulse is 45° instead of 90° as in conventional INEPT, which maximizes the polarization transfer for a two-spin order of p-H₂ (Eq. 2). However, phINEPT+ does not allow for a complete polarization transfer even for a simple AMX spin system. Optionally, one can modify it to have only selective pulses to improve the efficiency, which in some cases could enable complete polarization transfer.^[97]

The INEPT sequences were redesigned in the form of the ESOTHERIC (efficient spin order transfer to hetero nuclei via relayed inept chains) sequence,^[68,80,81] which uses only hard (broadband) pulses and theoretically allows for a 100% polarization transfer (Figure 2b). For example, this SOT sequence was used to prepare HP tracers for in vivo experiments.^[50] Also, other sequences, like alternating delays achieve polarization transfer (ADAPT)^[98,99] and others, were used in the PHIP context but not in PHIP-SAH systems yet.

It should be noted that the sequences discussed here are not specifically designed and used only for ¹³C PHIP-SAH—other nuclei were also successfully polarized like ¹⁵N in conventional PHIP^[100] or SABRE experiments^[30,101] where these sequences were used to measure *J* coupling constants^[102] or chemical exchange^[103–105] highlighting the importance of the SOT methods and their general utility.

There are many frequency-selective variants of such SOTs^[90,97,106] including relayed polarization transfer from p-H₂ to the neighboring protons^[92] or ¹³C^[60,62] and then to the final target ¹³C. The combination of ESOTHERIC and ¹³C-¹³C relayed polarization transfer is also referred to as maximizing insensitive nuclei enhancement reached via parahydrogen amplification (MINERVA).^[62,68] This polarization relay approach extended the scope of efficiently polarized PHIP-SAH tracers to those where direct p-H₂-to-¹³C interaction is negligible, like in allyl esters. Moreover, the use of a hard pulse on ¹³C channel with a variable flip angle allowed to control polarization transfer to the ¹³C-2 site in [1,2-¹³C₂]pyruvate-d₆: with a 90° pulse the polarization is completely transferred to the ¹³C-2 site, while with a 45° pulse, both sites are polarized but with the opposite phases.^[107]

4.4. Polarization via RF irradiation in a strong coupling regime (at low magnetic fields)

At low magnetic fields, the difference of Zeeman interactions between a magnetic field and the two protons originating from p-H₂ is negligible (the chemical shift difference in Hz is much less than the mutual *J* coupling). Therefore, despite the obvious chemical inequivalence of these protons in PHIP-SAH systems, they can be treated as chemically equivalent, making it possible to adapt RF sequences initially designed for spin systems with chemically equivalent protons at high fields^[108] for this case. In particular, adiabatic variation of these RF sequences can be employed.^[109]

Interestingly, ESOTHERIC-based SOT sequences, initially designed for the high-field case, can still be used at low fields if additional ¹³C labeling is introduced right

next to the triple bond where p-H₂ protons are added.^[62] This carbon (via the strong *J* coupling of 160 Hz) makes p-H₂ protons experience different magnetic fields even at low external fields, making sequence efficient at these conditions as well. In fact, more specialized sequences were designed for this purpose by Goldman et al.^[42,87] and Kadlecik et al.^[110] much earlier, although they have not yet been tested in the PHIP-SAH context.

4.5. Polarization transfer via magnetic field cycling

In addition to RF field-induced SOT, DC magnetic field cycling (MFC) is another efficient way to transfer polarization from p-H₂ to heteronuclei.^[111] This polarization transfer can be explained by the correlation of energy levels during the ramp of the magnetic field (Figure 2c). When the magnetic field reaches the energy level anti-crossing (LAC) of the singlet-state-populated levels of the two protons stemming from p-H₂, the heteronuclei can be hyperpolarized.^[112–114] This concept was adopted for PHIP-SAH^[48] and enabled polarization of pyruvate sufficient for in vitro spectroscopy^[115,116] and in vivo imaging.^[51]

Despite the progress in the development of MFC^[117–119] the levels of polarization achieved using the MFC approach for the PHIP-SAH system even theoretically are lower than in the case of RF SOT sequences. One of the reasons is the presence of numerous strong interactions between protons of a side arm. While at high field the deuteration^[55,68] or selective excitations^[90,106] reduce the number of spins involved in the process of polarization transfer, at low fields this is not the case, and deuteration can even be detrimental for efficient MFC.^[78]

4.6. Problems with spin order transfer methods

As with all SOT sequences, there is a large influence from imprecise settings, like RF pulse amplitude^[78] and erroneously determined *J* coupling constants,^[62,120] or when pH is very close to pKa of the molecule so that *J* coupling interactions are modulated^[43] or labile protons are exchanging.^[121,122]

Despite advances in catalysis^[123] and PHIP instrumentation,^[124] 100% polarization was not demonstrated on heteronuclei. One of the examples closest to the theoretical maximum was the hyperpolarization of ethyl [1-¹³C]acetate-d₆: after pairwise p-H₂ addition and application of ESOTHERIC RF SOT *P*_{13C} = 60.5% was achieved at ca. 1 mM concentration.^[80] Later, it was rationalized that a further increase in concentration results in effects that prevent the system from a further increase of molar polarization. The reason is that in the discussed SOT approaches (RF and MFC) it is assumed that the magnetic field of the sample itself is negligible. However, this is not the case when highly polarized spins are present. When the system has high magnetization (i.e., a high product of concentration and polarization), then nonlinear interactions of the sample with the NMR resonator (RF coil) affect the spin dynamics leading, among others, to a distant dipolar field^[125] (also referred to as demagnetization field^[126]), radiation damping,^[127] RASER^[128–132] and even intermolecular polarization transfer through dipolar interactions.^[132–134] All these lead to the reduced SOT efficacy. At the same time, RASER can offer interesting and unique opportunities

for investigating nonlinear systems and background-free detection of HP species.^[135–137]

Instead of using magnetization as a value with rather unhandy units, it is more practical to report molar polarization. So, Dagsys et al. demonstrated that their system-sample interaction prevented the generation of more than 60 mM ¹H molar polarization of dimethyl maleate.^[138] Several approaches were proposed to resolve the issue of high molar polarization of the sample: reduced field homogeneity,^[127] repetitive refocusing, bipolar pulsed field gradients,^[127] and implementing a Lee-Goldburg decoupling sequence.^[138–140] As the achieved molar polarization values are constantly increasing, the PHIP-SAH SOT techniques will be modified to compensate for such sample-resonator interactions, delivering polarization closer to the theoretical maximum.

5. Side arm removal and purification of hyperpolarized bolus

The next step after polarization is transferred to heteronuclei is the cleavage of the side arm, typically done using alkaline hydrolysis. Interestingly, this approach was first implemented in 2012 using PHIP-hyperpolarized ethyl acetate, aiming to obtain ¹H HP ethanol.^[141] However, hydrogenation occurred in D₂O, and removing the toxic catalyst was not attempted.

The first paper describing PHIP-SAH approach proposed a strategy for purification of hyperpolarized samples.^[48] According to this procedure, the corresponding unsaturated substrate is hydrogenated in an organic hydrophobic solvent (e.g., chloroform/methanol mixture) followed by SOT to carboxylic ¹³C nucleus in the product molecule (acetate or pyruvate). Then, an aqueous base (in the original paper, NaOD was used^[48]) is added to initiate (i) the cleavage of the side arm via hydrolysis and (ii) the phase separation in such a way that the homogeneous catalyst being retained in the organic phase, while the hyperpolarized target molecule (acetate or pyruvate sodium salts) is extracted in the aqueous phase. This approach was inspired by the previous work, in which sodium succinate in aqueous media was obtained via phase transfer.^[142] Finally, to produce a hyperpolarized sample with the physiological pH value (7.0–7.4), addition of a buffered acidic solution is needed.

The polarization level observed on the target carboxylate after hydrolysis of the HP ester depends on the maintenance of the ¹³C hyperpolarization during hydrolysis and phase extraction. In the next paper on the topic,^[54] the addition of sodium ascorbate to aqueous base solutions was suggested. It is assumed that such an oxygen scavenger would reduce the polarization losses for lactate caused by the paramagnetic impurities derived from catalyst degradation, which were identified using electron paramagnetic resonance spectroscopy.^[54] Later, the effect of adding sodium ascorbate on the ¹³C polarization losses was quantified:^[143] the observed P_{13C} of [1-¹³C]pyruvate increased from 3.4% to 5.2% when 50 mM ascorbate was added, accompanied by the increase of the ¹³C T₁ relaxation time at the Earth's

magnetic field from ca. 42 s to ca. 54 s. The ¹³C polarization of [1-¹³C]pyruvate, back-calculated to time zero, was estimated as 9.4 ± 0.5%, while the polarization level obtained on the allyl ester before side arm cleavage was 10 ± 1%, meaning that ¹³C hyperpolarization is almost intact during the hydrolysis and phase extraction steps.

The organic solvent used in the pioneering PHIP-SAH work^[48] was a chloroform/methanol mixture; the addition of methanol was motivated by the fact that it promotes hydrogenation via coordination to the intermediate Rh species in the catalytic cycle.^[74,75,144] To further improve the biological compatibility of the hyperpolarized tracer solution, it was first proposed to use ethanol instead of methanol,^[54] so hydrogenation was performed in chloroform/ethanol mixture (5:1). Later, the concentration of ethanol was first minimized,^[51] and then ethanol was completely removed from hydrogenation procedure.^[115,116] Chloroform is a non-coordinating solvent, and the activation of the catalyst precursor in chloroform (via hydrogenation of COD or NBD diene ligands) leads to the formation of non-catalytically active dimers;^[145] however, it was demonstrated that the active catalyst can be stabilized using unsaturated ester precursor^[75] directly. The series of cytotoxicity experiments^[116] performed on different prostate cancer cell lines (DU145 and PC3) indicates the beneficial effect of ethanol removal from the PHIP-SAH procedure on the cells' viability. Moreover, it was demonstrated that the aqueous solution of hyperpolarized [1-¹³C]pyruvate produced via the PHIP-SAH approach has moderate toxicity only after 24 h of incubation, and the toxicity appeared to be mainly caused by traces of chloroform while the hydrolysis side-product (allyl alcohol) did not affect cell viability after 24 h of incubation.

Chloroform is not miscible with water, but is still soluble to some extent (0.052 wt% at 293 K). The final concentration of chloroform in aqueous bolus of HP pyruvate was estimated as 30 ± 2 mM.^[75] The filtration of aqueous solution using a lipophilic resin was also tested;^[75] the chloroform concentration was thus reduced to 0.5 ± 0.1 mM, which is lower than the values recommended by Environmental Protection Agencies for water quality criteria.^[75]

Glöggl and coauthors^[62,107] presented another purification strategy for obtaining a biocompatible aqueous solution of HP metabolites via PHIP-SAH: the hydrogenation is carried out in a volatile organic solvent (acetone), which is miscible with water. In this case, the removal of the toxic solvent is achieved via evaporation, and Rh catalyst precipitates due to a low solubility in water. The residual concentration of acetone in aqueous phase was estimated as < 43 mM. The residual Rh concentration in the final solution was found to be below 45 μM by inductively coupled plasma mass spectroscopy (ICP-MS) analysis, which corresponds to a 150-fold reduction from the value in the starting solution.

A similar approach was utilized in the work of Nagel et al.^[49] hydrogenation of unsaturated pyruvate precursor took place in acetone-d₆ followed by SOT to ¹³C (driven by RF irradiation at a 100 μT field), and then sodium hydroxide was added to initiate the cleavage of the hydrogenated side arm moiety; however, the phase

separation of the organic and the aqueous phase was then initiated with the addition of methyl *tert*-butyl ether (MTBE). Moreover, the side arm of the ester was specially designed for poor water solubility, making the purification process via phase extraction after cleavage more efficient. Such a purification process significantly reduces Rh and acetone concentration in the produced HP sample: the residual Rh and acetone concentrations were $117 \pm 10 \mu\text{M}$ and $90 \pm 17 \text{ mM}$, respectively. As a result, a sample of 70–160 mM [^{13}C]pyruvate with $P_{^{13}\text{C}} \approx 18\%$ with a volume of up to 2 mL was produced.^[49]

Another possibility for producing catalyst-free aqueous solutions of hyperpolarized tracer is to perform hydrogenation in water using heterogeneous catalysts that can be easily filtered. Using this approach, ^{13}C hyperpolarization was obtained for ethyl acetate^[71,100,146] via heterogeneous hydrogenation of vinyl acetate in aqueous medium over a solid catalyst. However, heterogeneous catalysts are inferior to homogeneous ones in the preservation of singlet order of $p\text{-H}_2$ in the hydrogenated products: supported Rh/TiO₂ catalyst provided $P_{^{13}\text{C}}$ of only ca. 0.1% for ethyl acetate.^[71] The specially designed Pd^[147] or Rh^[100] ligand-stabilized nanocatalysts provide higher ^{13}C polarization levels for ethyl acetate (0.2 and 1.3%, respectively), but at the cost of very low chemical conversion. The same Rh nanocatalyst (N-acetyl cysteine decorated Rh nanoparticles) was used for PHIP-SAH of α -amino acids^[148] (glycine and alanine) directly in aqueous solutions via hydrogenation of corresponding vinyl esters. Moreover, hyperpolarized sodium salts of glycine and alanine were obtained via hydrolysis with NaOD, and the observed $P_{^{13}\text{C}}$ levels of ^{13}C carboxylic sites were 0.29 and 0.25% for the free glycine and alanine, respectively.

6. In vitro and in vivo applications

Ultimately, the main goal of the PHIP-SAH technique is the hyperpolarization of biomolecules for further detection and quantification of signal-enhanced metabolites in vitro and in vivo. As of today, in vitro and in vivo applications of PHIP-SAH are mostly limited to pyruvate, which is not unexpected considering the crucial role of pyruvate in cellular metabolism and, in particular, the presence of pyruvate metabolism disorders in unhealthy tissues, and impressive clinical studies pioneered with dDNP.^[32,33] Pyruvate is the terminal product of glycolysis and can then undergo several metabolic transformations: transamination into alanine catalyzed by alanine transaminase (ALT), reduction into lactate catalyzed by lactate dehydrogenase (LDH), and decarboxylation into acetyl-CoA by pyruvate dehydrogenase complex (PDC). The rates of these reactions strongly depend on the cellular conditions as a whole, particularly the redox potential and the oxygen concentration. It is widely known that cancer cells have altered metabolism, in particular, acidic extracellular pH, increased glucose uptake, and increased production of lactate (this is referred to as the Warburg effect^[149,150]). These hallmarks of cancer cell metabolism are used to diagnose a wide range of tumor types.^[33,151] In terms of diagnostic specificity, magnetic resonance spectroscopic

imaging (MRSI) along with ^{13}C -hyperpolarized pyruvate administration is of particular interest, since it allows monitoring the pyruvate-to-lactate conversion and mapping LDH activity.^[32]

In vitro applications of PHIP-SAH-HP compounds typically involve either following the kinetics of their enzymatic or nonenzymatic transformations or metabolic studies in cell lines. For example, PHIP-SAH ^{13}C -hyperpolarized pyruvate was used to investigate the kinetic parameters of LDH-catalyzed conversion of pyruvate into lactate.^[115] The same group of authors also performed a similar study using HP [^{13}C]lactate in a backward enzymatic reaction, i.e., oxidation of lactate to pyruvate catalyzed by LDH.^[54] Later, Korchak et al. demonstrated the possibility of observing enzymatic pyruvate-to-lactate conversion at a low 24 mT magnetic field using HP [^{13}C]pyruvate- d_3 .^[61] Using a ^{13}C nucleus in position 2, they could distinguish pyruvate and lactate at this low field with negligible chemical shift difference due to strong $^1J_{\text{CH}}$ coupling in [^{13}C]lactate- d_3 . Recently, it was shown^[107] that HP [$^{13}\text{C}_2$]pyruvate- d_3 can also be used to monitor nonenzymatic reaction of pyruvate with H₂O₂. The formation of acetate, carbon dioxide, carbonate, and bicarbonate products was demonstrated. Moreover, the detection of 2-hydroperoxy-2-hydroxypropanoate intermediate of this reaction was made possible through NMR hyperpolarization. Later, it was shown that the HP H¹³CO₃⁻/¹³CO₂ pair formed in this reaction can be used as a pH sensor.^[152]

Concerning in cell studies, Mamone et al. demonstrated the possibility of the real-time monitoring of pyruvate-to-lactate conversion in HeLa cells, a prototypical cancer cell line, using HP [^{13}C]pyruvate.^[62] It was also shown that HP [^{13}C]pyruvate metabolic conversion can be used for assessing the cancer cell lines aggressiveness. In particular, Reineri and co-workers used PHIP-SAH-HP [^{13}C]pyruvate to study two breast cancer cell lines (168FARN and 4T1)^[115] and three prostate cancer cell lines (DU145, PC3, and LnCap).^[116] Both works showed that the rate of pyruvate-to-lactate conversion strongly depends on the aggressiveness of the cell line (Figure 3) and on the state of cells (intact or lysed). PHIP-SAH-hyperpolarized [^{13}C]pyruvate- d_3 has been used for investigations of Hodgkin lymphoma cancer cell line (L1236).^[153] It was demonstrated that the anti-cancer therapeutic FK866 (inhibitor of nicotinamide phosphoribosyltransferase) significantly reduces the rate of pyruvate-to-lactate conversion. This inhibition effect can be recovered by supplying the cells with NADH, allowing for performing two consecutive measurements on the same cell sample.^[153] HP [^{13}C]pyruvate- d_3 was also used to study cellular models of Parkinson's disease.^[68] This work examined the effect of α -synuclein protein expression on the rate of pyruvate-to-lactate conversion, and it was shown that HEK 293T cell line with overexpression of α -synuclein gene had twice the rate of conversion in comparison with the cell line in which α -synuclein gene was knocked out. Also, this work demonstrated the feasibility of combining protein structure determination and metabolic analysis on the same cell sample. It is important to note that HP [^{13}C]pyruvate can be used to study LDH activity in intact

cells in contrast to conventional biochemical assay. Hyperpolarization is noninvasive and enables for a

multiple administration and analysis of cells and organoids that is useful for longitudinal studies.^[154,155]

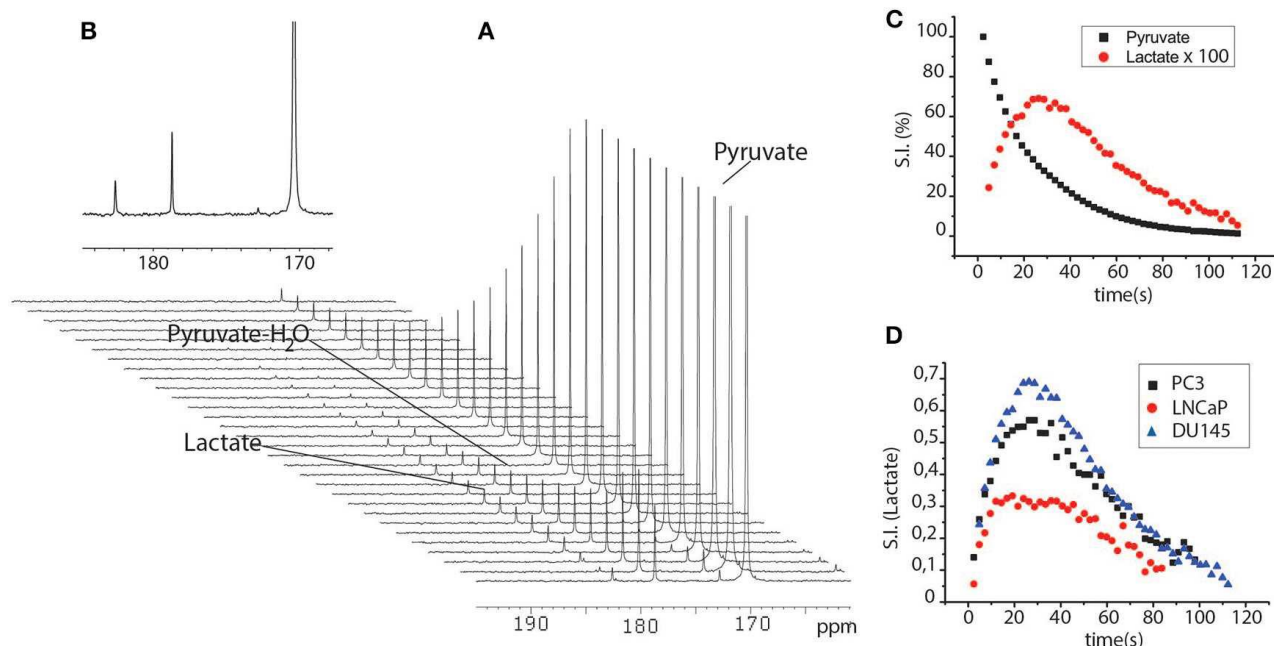


Figure 3. (A) A series of ¹³C NMR spectra acquired after the perfusion of a cell suspension (10M PC3 cells) with the aqueous solution of HP [1-¹³C]pyruvate. Spectra were acquired using a small flip angle pulse (18°) and 2 s delays between the scans. (B) An expanded ¹³C NMR spectrum at the maximum intensity of the lactate signal. (C) Time-dependent pyruvate and lactate curves obtained from the integrals of the signals of the two metabolites in the ¹³C NMR spectra reported in (A). (D) Time-dependent lactate curves obtained after adding HP [1-¹³C]pyruvate to a suspension of DU145, PC3, and LNCaP cells. Adapted from Ref. ^[116] published under a Creative Commons Attribution 4.0 International License (CC BY 4.0) by Frontiers Media.

Another application of hyperpolarized tracers is in vivo MRI visualization of tumors. For the first time, the feasibility of using PHIP-SAH-HP [1-¹³C]pyruvate for in vivo metabolic imaging was demonstrated by Cavallari et al. in 2018.^[51] The possibility of detection of metabolic disorders before the development of the disease was demonstrated on a mouse model of dilated cardiomyopathy. For genetically modified *Lmna* mice (mutations lead to several diseases, particularly cardiomyopathy), the reduced rate of pyruvate-to-lactate conversion was observed compared with a control wild-type line. Subsequent studies examined the rate of pyruvate-to-lactate conversion using hyperpolarized [1-¹³C]pyruvate-*d*₃ in human cancer xenografts: melanoma,^[50] pancreatic and colon^[156] tumors. These works showed that the pyruvate-to-lactate conversion can be monitored in vivo along with its kinetics in real time (Figure 4). Moreover, the different rates were observed for various types of tumors,^[156] which is important for potential diagnostics and tumor grading.

Also, Hune et al.^[157] demonstrated the possibility of using HP [1-¹³C]pyruvate to study multiple organs in separate injections to determine the rate of pyruvate-to-lactate conversion in these organs in vivo in mice. This approach allows to investigate the relationship between metabolism in different regions of the body of the same animal and to reduce the number of animals used in biological studies, which is important for further scaling of such studies and a way to go for a whole body molecular MRI.

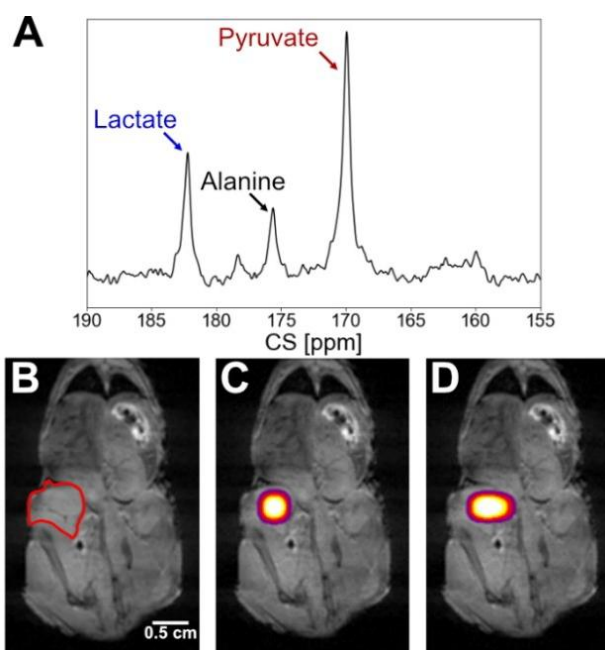


Figure 4. (A) Single scan ¹³C NMR spectrum acquired with a 10° pulse 10 s after the injection of HP [1-¹³C]pyruvate-*d*₃ into melanoma tumor-bearing mouse. (B) Anatomical ¹H image with the tumor region indicated in red. (C) ¹³C pyruvate image and (D) lactate image in the tumor region. The image is acquired 20 s after the injection. Adapted from Ref. ^[50] published under a Creative Commons Attribution-Noncommercial 4.0 International License (CC BY-NC 4.0) by Wiley-VCH GmbH.

One of the key questions raised regarding the potential use of the PHIP-SAH approach in biological research is its comparison with the dDNP method in the context of in vivo applications. Recently,^[49] [1-¹³C]pyruvate hyperpolarized using PHIP-SAH approach in an automated hyperpolarizer was benchmarked in the in vivo 3D metabolic MRI against [1-¹³C]pyruvate

hyperpolarized with a commercial dDNP device. Eventually, it was shown that safety profile, image quality and the measured rate of pyruvate-to-lactate conversion are equivalent for PHIP and dDNP approaches (Figure 5). Thus, this work proves that the PHIP-SAH method is a strong alternative candidate to established dDNP in the context of biological studies.

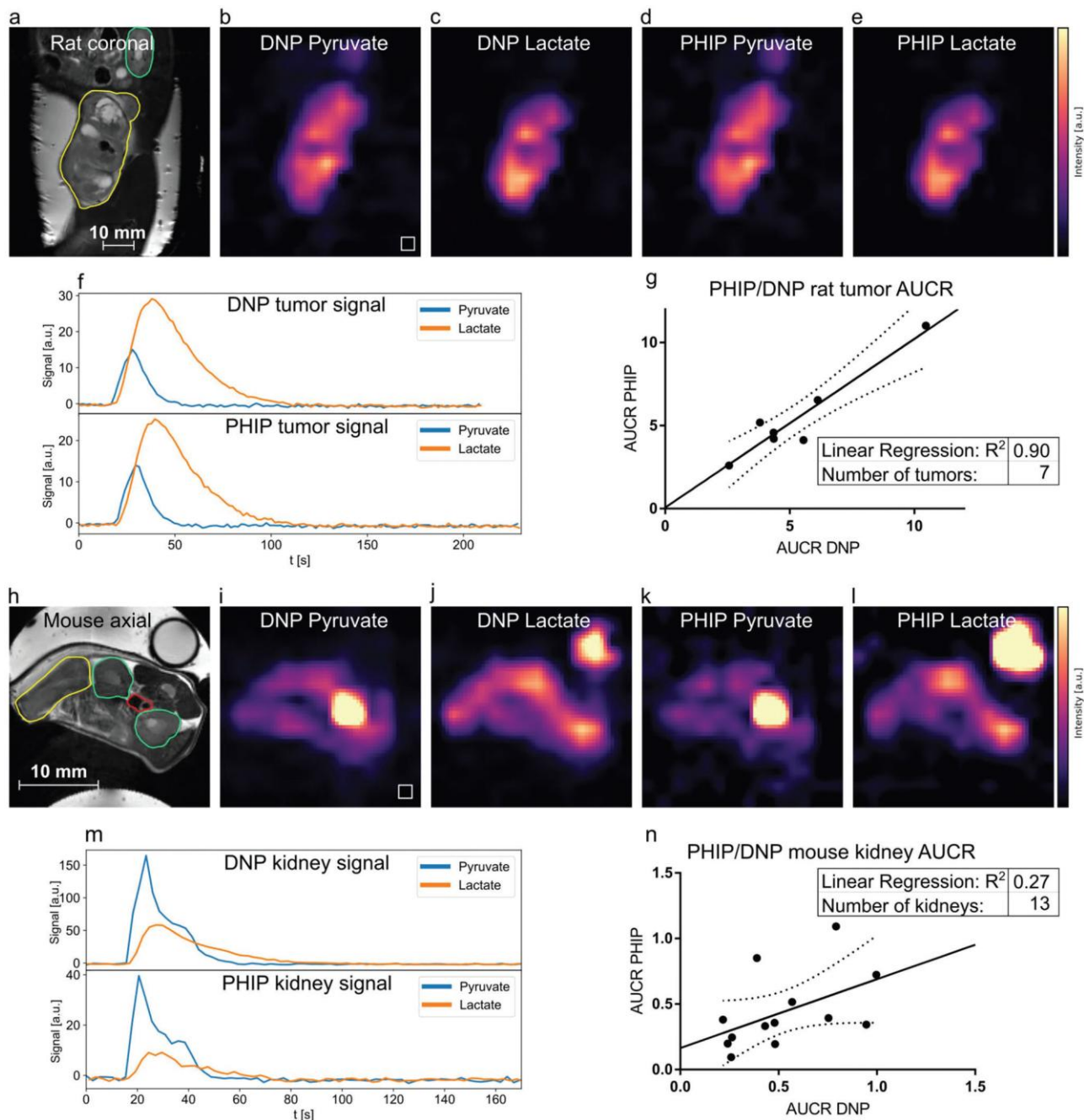


Figure 5. Comparison of metabolism in rat tumors and mice kidneys between PHIP-SAH and dDNP HP [1-¹³C]pyruvate using a dual metabolite targeted spectrally-selective bSSFP sequence. (a–f): PHIP-SAH and dDNP datasets of a Mat B III tumor-bearing rat showing the distribution of injected HP [1-¹³C]pyruvate (b,d) and lactate (c,e). In the corresponding anatomical reference (a), the tumor and kidney are drawn in yellow and green, respectively. The tumor 3D ROI pyruvate and lactate time curves are shown in (f). (g): A comparison of rat tumor area-under-the-curve-ratio (AUCR) values of PHIP-SAH and dDNP shows a very good correlation between the two methods ($R^2 = 0.90$). (h–l): pyruvate and lactate distributions in a tumor-bearing mouse are shown, with the corresponding anatomical reference in (h). Tumor (yellow), kidneys (green), and blood vessel (red) ROIs are depicted. A [1-¹³C]lactate phantom for RF power calibration is visible in the top right of the panels (h,j,l). (m): signal intensity time curves from the left kidney (green ROI). (n): correlation of PHIP-SAH and dDNP AUCRs of mouse kidneys ($R^2 = 0.27$). Dashed lines in (g,n) indicate the 95% confidence interval. The signal intensities in (b,c,d,e,i,j,k,l) were scaled to maximum value for better

comparability. Adapted from Ref. [49] published under a Creative Commons Attribution 4.0 International License (CC BY 4.0) by Wiley-VCH GmbH.

It is important to note that although almost all of the described in vitro and in vivo studies focused on the use of HP pyruvate, there are no fundamental limitations on the use of other PHIP-SAH-HP carboxylate biomolecules, e.g., acetate, α -ketoglutarate, and others. Therefore, we envision using this method to hyperpolarize a wide range of biomolecules for further in vitro and in vivo studies in the near future.

7. Summary and outlook

To summarize, the PHIP-SAH approach has enjoyed a rapid development over the past 10 years since the introduction of this concept by Reineri et al. [48]. Significant improvements were made in developing SOT methods and the synthetic design of PHIP-SAH precursors, including tailored isotopic labeling. As a result, the attainable polarizations were increased up to ca. 60% for products of pairwise parahydrogen addition [68] and up to ca. 37% for the purified carboxylate after side arm cleavage and purification of an HP

sample [152] (see Table 2 for a summary of achieved polarizations for pyruvate). The molar polarization of [1- ^{13}C]pyruvate as high as 29 mM has been reported. [49]

One can envision several possible directions of future advances in PHIP-SAH. First of all, HP pyruvate production efficiency can be further increased, mainly via engineering optimization of all PHIP-SAH steps, which was rarely done in research settings. Second, the PHIP-SAH approach can be advanced to other biologically important carboxylates beyond pyruvate. Moreover, other heteronuclei, e.g., ^{15}N or ^{31}P , can be hyperpolarized via PHIP-SAH—a pilot study with phosphate esters was recently reported by Zlobina et al. [158]

Altogether, the recent advances positioned the PHIP-SAH approach as a viable alternative to the dDNP method, which is already well-established in clinical studies. As PHIP-SAH is more affordable and has a higher throughput than dDNP, we expect that this approach will pave the way for clinical applications in the coming years.

Table 2. The achieved ^{13}C polarization levels (% and molar) of pyruvate in published literature (grouped by the used SOT methods (RF at high field / RF at low field / MFC) and substrate). N/A = data are not available.

PHIP-SAH product	SOT method	$P_{^{13}\text{C}}$ after SOT		$P_{^{13}\text{C}}$ after cleavage and purification		Ref.
		$P_{^{13}\text{C}}$, %	Molar $P_{^{13}\text{C}}$, mM	$P_{^{13}\text{C}}$, %	Molar $P_{^{13}\text{C}}$, mM	
Ethyl [1- ^{13}C]pyruvate- d_6	ESOTHERIC	14	14	—	—	[78]
Ethyl [1- ^{13}C]pyruvate- d_6	MINERVA	60 ± 3	7.8 ± 0.4	27 ± 1	3.5 ± 0.1	[68]
Ethyl [1- ^{13}C]pyruvate- d_6	MINERVA	53 ± 2	$27 \pm 1^{\text{a}}$	12 ± 4	$8 \pm 3^{\text{a}}$	[50]
Ethyl [1- ^{13}C]pyruvate- d_6	MINERVA	N/A	N/A	36.65 ± 0.06	14.66 ± 0.02	[152]
Ethyl [2- ^{13}C]pyruvate- d_6	MINERVA	10.7 ± 0.7	1.07 ± 0.07	3.9 ± 0.4	0.39 ± 0.04	[68]
Ethyl [1,2- $^{13}\text{C}_2$]pyruvate- d_6	MINERVA	$24.4 \pm 0.4^{\text{b}}$ $-24 \pm 2^{\text{c}}$	$2.44 \pm 0.04^{\text{b}}$ $-2.4 \pm 0.2^{\text{c}}$	$6.5 \pm 0.4^{\text{b}}$ $-7 \pm 1^{\text{c}}$	$0.65 \pm 0.04^{\text{b}}$ $-0.7 \pm 0.1^{\text{c}}$	[68]
But-3-en-2-yl- d_4 [1- ^{13}C]pyruvate	^1H -relayed ESOTHERIC	7.1 ± 0.4	0.18 ± 0.01	4.3 ± 0.2	0.043 ± 0.002	[92]
<i>Cis</i> -[2- ^{13}C]cinnamyl-1- d_2 [1- ^{13}C]pyruvate	MINERVA	24	13	8	0.96	[62]
<i>Cis</i> -[1- ^{13}C]cinnamyl-1- d_2 [1- ^{13}C]pyruvate	MINERVA	14 ± 2	$8 \pm 1^{\text{a}}$	N/A	N/A	[153]
<i>Cis</i> -[1- ^{13}C]cinnamyl [1- ^{13}C]pyruvate- d_{10}	MINERVA	17.4 ± 0.6	1.74 ± 0.06	8.6 ± 0.7	0.86 ± 0.07	[68]
<i>Cis</i> -[2- ^{13}C]cinnamyl- d_7 [1- ^{13}C]pyruvate	MINERVA	14.5	N/A	6.5	2.6	[157]
<i>Cis</i> -[1- ^{13}C]cinnamyl [2- ^{13}C]pyruvate- d_{10}	ESOTHERIC	25 ± 2	10.9 ± 0.9	$10.1 \pm 0.1^{\text{d}}$	$2.22 \pm 0.02^{\text{d}}$	[61]
<i>Cis</i> -cinnamyl-1- d [1- ^{13}C]pyruvate	B_1 sweep @ 100 μT	9.8	3.5	—	—	[109]
<i>Cis</i> -(4- <i>tert</i> -butoxycarbonyl)prop-2-enyl-1- d_2 [1- ^{13}C]pyruvate	B_1 sweep @ 100 μT	N/A	N/A	18 ± 1	29	[49]
Ethyl [1- ^{13}C]pyruvate	MFC	3.8 ± 0.3	2.1 ± 0.2	—	—	[67]
Allyl [1- ^{13}C]pyruvate	MFC	8.3 ± 0.7	$6.3 \pm 0.5^{\text{a}}$	5.2 ± 0.2	N/A	[143]
Allyl [1- ^{13}C]pyruvate	MFC	6.2 ± 0.3	N/A	3.5 ± 0.5	1.2 ± 0.2	[51]
Allyl [1- ^{13}C]pyruvate	MFC	6.2 ± 0.3	3.5 ± 0.2	—	—	[67]
Allyl [1- ^{13}C]pyruvate	MFC	$8.4 \pm 0.6^{\text{e}}$ $5.2 \pm 0.6^{\text{f}}$	$6.0 \pm 0.4^{\text{e}}$ $4.0 \pm 0.5^{\text{f}}$	$3.4 \pm 0.6^{\text{e}}$ $2.2 \pm 0.3^{\text{f}}$	$1.7 \pm 0.3^{\text{e}}$ $0.66 \pm 0.09^{\text{f}}$	[75]

^aCalculated assuming 100% conversion (actual conversion is not reported). ^b1- ^{13}C site. ^c2- ^{13}C site. ^dAfter side arm cleavage but

without purification. ^eIn 95:5 toluene/ethanol mixture. ^fIn CDCl₃.

Acknowledgements

O.G.S., N.V.C., D.B.B., and S.V.S. thank the Russian Science Foundation (grant 24-73-10093) for the support of preparation of all sections of this review except Section 4: Polarization transfer to heteronuclei. A.N.P. and J.B.H. acknowledge support from German Federal Ministry of Education and Research (BMBF) within the framework of the e:Med research and funding concept (01ZX1915C, 03WIR6208A hyperquant), DFG (555951950, 527469039, 469366436, HO-4602/2-2, HO-4602/3, HO-4602/4, EXC2167, FOR5042, TRR287). MOIN CC was founded by a grant from the European Regional Development Fund (ERDF) and the Zukunftsprogramm Wirtschaft of Schleswig-Holstein (Project no. 122-09-053).

Keywords: NMR spectroscopy • hyperpolarization • PHIP • parahydrogen • magnetic resonance imaging

References

- [1] J. Eills, D. Budker, S. Cavagnero, E. Y. Chekmenev, S. J. Elliott, S. Jannin, A. Lesage, J. Matysik, T. Meersmann, T. Prisner, J. A. Reimer, H. Yang, I. V. Koptuyug, *Chem. Rev.* **2023**, *123*, 1417–1551.
- [2] P. Berthault, C. Boutin, C. Martineau-Corcoss, G. Carret, *Prog. Nucl. Magn. Reson. Spectrosc.* **2020**, *118–119*, 74–90.
- [3] V. Ribay, C. Praud, M. P. M. Letertre, J.-N. Dumez, P. Giraudeau, *Curr. Opin. Chem. Biol.* **2023**, *74*, 102307.
- [4] J. G. Skinner, L. Menichetti, A. Flori, A. Dost, A. B. Schmidt, M. Plaumann, F. A. Gallagher, J.-B. Hövener, *Mol. Imaging Biol.* **2018**, *20*, 902–918.
- [5] M. Negroni, D. Kurzbach, *ChemBioChem* **2023**, *24*, e202200703.
- [6] M. Vaeggemose, R. F. Schulte, C. Laustsen, *Metabolites* **2021**, *11*, 219.
- [7] N. J. Stewart, S. Matsumoto, *Magn. Reson. Med. Sci.* **2021**, *20*, 1–17.
- [8] D. A. Barskiy, A. M. Coffey, P. Nikolaou, D. M. Mikhaylov, B. M. Goodson, R. T. Branca, G. J. Lu, M. G. Shapiro, V.-V. Telkki, V. V. Zhivonitko, I. V. Koptuyug, O. G. Salnikov, K. V. Kovtunov, V. I. Bukhtiyarov, M. S. Rosen, M. J. Barlow, S. Safavi, I. P. Hall, L. Schröder, E. Y. Chekmenev, *Chem. – Eur. J.* **2017**, *23*, 725–751.
- [9] A. S. Khan, R. L. Harvey, J. R. Birchall, R. K. Irwin, P. Nikolaou, G. Schrank, K. Emami, A. Dummer, M. J. Barlow, B. M. Goodson, E. Y. Chekmenev, *Angew. Chem. Int. Ed.* **2021**, *60*, 22126–22147.
- [10] H. Marshall, N. J. Stewart, H.-F. Chan, M. Rao, G. Norquay, J. M. Wild, *Prog. Nucl. Magn. Reson. Spectrosc.* **2021**, *122*, 42–62.
- [11] L. Sellies, I. Reile, R. L. E. G. Aspers, M. C. Feiters, F. P. J. T. Rutjes, M. Tessari, *Chem. Commun.* **2019**, *55*, 7235–7238.
- [12] T. Biedenbänder, V. Aladin, S. Saeidpour, B. Corzilius, *Chem. Rev.* **2022**, *122*, 9738–9794.
- [13] W. Y. Chow, G. De Paëpe, S. Hediger, *Chem. Rev.* **2022**, *122*, 9795–9847.
- [14] S. B. Duckett, N. J. Wood, *Coord. Chem. Rev.* **2008**, *252*, 2278–2291.
- [15] A. N. Pravdivtsev, B. J. Tickner, S. Glöggler, J.-B. Hövener, G. Buntkowsky, S. B. Duckett, C. R. Bowers, V. V. Zhivonitko, *ArXiv* **2024**, DOI: 10.48550/arXiv.2409.19108.
- [16] E. V. Pokochueva, D. B. Burueva, O. G. Salnikov, I. V. Koptuyug, *ChemPhysChem* **2021**, *22*, 1421–1440.
- [17] K. V. Kovtunov, V. V. Zhivonitko, I. V. Skovpin, D. A. Barskiy, I. V. Koptuyug, *Top. Curr. Chem.* **2013**, *338*, 123–180.
- [18] C.-H. Chen, W.-C. Shih, C. Hilty, *J. Am. Chem. Soc.* **2015**, *137*, 6965–6971.
- [19] T. Kobayashi, F. A. Perras, I. I. Slowing, A. D. Sadow, M. Pruski, *ACS Catal.* **2015**, *5*, 7055–7062.
- [20] W.-C. Liao, B. Ghaffari, C. P. Gordon, J. Xu, C. Copéret, *Curr. Opin. Colloid Interface Sci.* **2018**, *33*, 63–71.
- [21] I. B. Moroz, M. Leskes, *Annu. Rev. Mater. Res.* **2022**, *52*, 25–55.
- [22] S. Haber, M. Leskes, *Solid State Nucl. Magn. Reson.* **2022**, *117*, 101763.
- [23] M. M. Chaumeil, J. A. Bankson, K. M. Brindle, S. Epstein, F. A. Gallagher, M. Grashei, C. Guglielmetti, J. D. Kaggie, K. R. Keshari, S. Knecht, C. Laustsen, A. B. Schmidt, D. Vigneron, Y.-F. Yen, F. Schilling, *Mol. Imaging Biol.* **2024**, *26*, 222–232.
- [24] H. Park, Q. Wang, *Chem. Sci.* **2022**, *13*, 7378–7391.
- [25] J. H. Ardenkjær-Larsen, B. Fridlund, A. Gram, G. Hansson, L. Hansson, M. H. Lerche, R. Servin, M. Thaning, K. Golman, *Proc. Natl. Acad. Sci. U. S. A.* **2003**, *100*, 10158–10163.
- [26] S. J. Elliott, Q. Stern, M. Ceillier, T. El Daraï, S. F. Cousin, O. Cala, S. Jannin, *Prog. Nucl. Magn. Reson. Spectrosc.* **2021**, *126–127*, 59–100.
- [27] A. C. Pinon, A. Capozzi, J. H. Ardenkjær-Larsen, *Magn. Reson. Mater. Phys. Biol. Med.* **2021**, *34*, 5–23.
- [28] C. R. Bowers, D. P. Weitekamp, *J. Am. Chem. Soc.* **1987**, *109*, 5541–5542.
- [29] T. C. Eischenschmid, R. U. Kirss, P. P. Deutsch, S. I. Hommeltoft, R. Eisenberg, J. Bargon, R. G. Lawler, A. L. Balch, *J. Am. Chem. Soc.* **1987**, *109*, 8089–8091.
- [30] R. W. Adams, J. A. Aguilar, K. D. Atkinson, M. J. Cowley, P. I. P. Elliott, S. B. Duckett, G. G. R. Green, I. G. Khazal, J. López-Serrano, D. C. Williamson, *Science* **2009**, *323*, 1708–1711.
- [31] O. G. Salnikov, D. B. Burueva, I. V. Skovpin, I. V. Koptuyug, *Mendeleev Commun.* **2023**, *33*, 583–596.
- [32] S. J. Nelson, J. Kurhanewicz, D. B. Vigneron, P. E. Z. Larson, A. L. Harzstark, M. Ferrone, M. van Criekinge, J. W. Chang, R. Bok, I. Park, G. Reed, L. Carvajal, E. J. Small, P. Munster, V. K. Weinberg, J. H. Ardenkjær-Larsen, A. P. Chen, R. E. Hurd, L.-I.

- Odegardstuen, F. J. Robb, J. Tropp, J. A. Murray, *Sci. Transl. Med.* **2013**, *5*, 198ra108.
- [33] J. Kurhanewicz, D. B. Vigneron, J. H. Ardenkjaer-Larsen, J. A. Bankson, K. Brindle, C. H. Cunningham, F. A. Gallagher, K. R. Keshari, A. Kjaer, C. Laustsen, D. A. Mankoff, M. E. Merritt, S. J. Nelson, J. M. Pauly, P. Lee, S. Ronen, D. J. Tyler, S. S. Rajan, D. M. Spielman, L. Wald, X. Zhang, C. R. Malloy, R. Rizi, *Neoplasia* **2019**, *21*, 1–16.
- [34] C. H. Cunningham, J. Y. C. Lau, A. P. Chen, B. J. Geraghty, W. J. Perks, I. Roifman, G. A. Wright, K. A. Connelly, *Circ. Res.* **2016**, *119*, 1177–1182.
- [35] M. J. Albers, R. Bok, A. P. Chen, C. H. Cunningham, M. L. Zierhut, V. Y. Zhang, S. J. Kohler, J. Tropp, R. E. Hurd, Y.-F. Yen, S. J. Nelson, D. B. Vigneron, J. Kurhanewicz, *Cancer Res.* **2008**, *68*, 8607–8615.
- [36] C. R. Bowers, D. P. Weitekamp, *Phys. Rev. Lett.* **1986**, *57*, 2645–2648.
- [37] M. G. Pravica, D. P. Weitekamp, *Chem. Phys. Lett.* **1988**, *145*, 255–258.
- [38] D. A. Barskiy, S. Knecht, A. V. Yurkovskaya, K. L. Ivanov, *Prog. Nucl. Magn. Reson. Spectrosc.* **2019**, *114–115*, 33–70.
- [39] A. N. Pravdivtsev, A. V. Yurkovskaya, H.-M. Vieth, K. L. Ivanov, R. Kaptein, *ChemPhysChem* **2013**, *14*, 3327–3331.
- [40] T. Theis, M. Truong, A. M. Coffey, E. Y. Chekmenev, W. S. Warren, *J. Magn. Reson.* **2014**, *248*, 23–26.
- [41] S. Wagner, *Magn. Reson. Mater. Phys. Biol. Med.* **2014**, *27*, 195–199.
- [42] M. Goldman, H. Jóhannesson, O. Axelsson, M. Karlsson, *C. R. Chim.* **2006**, *9*, 357–363.
- [43] E. Y. Chekmenev, J. Hövener, V. A. Norton, K. Harris, L. S. Batchelder, P. Bhattacharya, B. D. Ross, D. P. Weitekamp, *J. Am. Chem. Soc.* **2008**, *130*, 4212–4213.
- [44] J.-B. Hövener, E. Y. Chekmenev, K. C. Harris, W. H. Perman, T. T. Tran, B. D. Ross, P. Bhattacharya, *Magn. Reson. Mater. Phys. Biol. Med.* **2009**, *22*, 123–134.
- [45] A. N. Pravdivtsev, G. Buntkowsky, S. B. Duckett, I. V. Koptyug, J.-B. Hövener, *Angew. Chem. Int. Ed.* **2021**, *60*, 23496–23507.
- [46] M. Körner, G. Sauer, A. Heil, D. Nasu, M. Empting, D. Tietze, S. Voigt, H. Weidler, T. Gutmann, O. Avrutina, H. Kolmar, T. Ratajczyk, G. Buntkowsky, *Chem. Commun.* **2013**, *49*, 7839–7841.
- [47] G. Sauer, D. Nasu, D. Tietze, T. Gutmann, S. Englert, O. Avrutina, H. Kolmar, G. Buntkowsky, *Angew. Chem. Int. Ed.* **2014**, *53*, 12941–12945.
- [48] F. Reineri, T. Boi, S. Aime, *Nat. Commun.* **2015**, *6*, 5858.
- [49] L. Nagel, M. Gierse, W. Gottwald, Z. Ahmadova, M. Grashei, P. Wolff, F. Josten, S. Karaali, C. A. Müller, S. Lucas, J. Scheuer, C. Müller, J. Blanchard, G. J. Topping, A. Wendlinger, N. Setzer, S. Sühnel, J. Handwerker, C. Vassiliou, F. H. A. van Heijster, S. Knecht, M. Keim, F. Schilling, I. Schwartz, *Adv. Sci.* **2023**, *10*, 2303441.
- [50] T. Hune, S. Mamone, H. Schroeder, A. P. Jagtap, S. Sternkopf, G. Stevanato, S. Korchak, C. Fokken, C. A. Müller, A. B. Schmidt, D. Becker, S. Glöggler, *ChemPhysChem* **2023**, *24*, e202200615.
- [51] E. Cavallari, C. Carrera, M. Sorge, G. Bonne, A. Muchir, S. Aime, F. Reineri, *Sci. Rep.* **2018**, *8*, 8366.
- [52] M. Mishkovsky, A. Comment, *Anal. Biochem.* **2017**, *529*, 270–277.
- [53] M. Pedersen, S. Ursprung, J. D. Jensen, B. Jespersen, F. Gallagher, C. Laustsen, *Magn. Reson. Mater. Phys. Biol. Med.* **2020**, *33*, 23–32.
- [54] E. Cavallari, C. Carrera, S. Aime, F. Reineri, *Chem. – Eur. J.* **2017**, *23*, 1200–1204.
- [55] A. Brahms, A. N. Pravdivtsev, L. Thorns, F. D. Sönnichsen, J.-B. Hövener, R. Herges, *J. Org. Chem.* **2023**, *88*, 15018–15028.
- [56] D. B. Burueva, S. V. Sviyazov, N. V. Chukanov, N. R. Mustafin, O. G. Salnikov, E. Y. Chekmenev, K. V. Kovtunov, I. V. Koptyug, *J. Magn. Reson. Open* **2024**, *21*, 100176.
- [57] N. V. Chukanov, O. G. Salnikov, R. V. Shchepin, K. V. Kovtunov, I. V. Koptyug, E. Y. Chekmenev, *ACS Omega* **2018**, *3*, 6673–6682.
- [58] A. P. Jagtap, S. Mamone, S. Glöggler, *Magn. Reson. Chem.* **2023**, *61*, 674–680.
- [59] M.-J. Ferrer, E. L. Kuker, E. Semenova, A. J. Gangano, M. P. Lapak, A. J. Grenning, V. M. Dong, C. R. Bowers, *J. Am. Chem. Soc.* **2022**, *144*, 20847–20853.
- [60] S. Korchak, S. Yang, S. Mamone, S. Glöggler, *ChemistryOpen* **2018**, *7*, 344–348.
- [61] S. Korchak, A. P. Jagtap, S. Glöggler, *Chem. Sci.* **2021**, *12*, 314–319.
- [62] S. Mamone, A. P. Jagtap, S. Korchak, Y. Ding, S. Sternkopf, S. Glöggler, *Angew. Chem. Int. Ed.* **2022**, *61*, e202206298.
- [63] J. Ziriakus, T. K. Zimmermann, A. Pöthig, M. Drees, S. Haslinger, D. Jantke, F. E. Kühn, *Adv. Synth. Catal.* **2013**, *355*, 2845–2859.
- [64] A. A. Ketterling, A. S. Lisitsyn, A. V. Nosov, V. A. Likholobov, *Appl. Catal.* **1990**, *66*, 123–131.
- [65] R. V. Shchepin, D. A. Barskiy, A. M. Coffey, I. V. Manzanera Esteve, E. Y. Chekmenev, *Angew. Chem. Int. Ed.* **2016**, *55*, 6071–6074.
- [66] E. Cavallari, C. Carrera, T. Boi, S. Aime, F. Reineri, *J. Phys. Chem. B* **2015**, *119*, 10035–10041.
- [67] C. Carrera, E. Cavallari, G. Digilio, O. Bondar, S. Aime, F. Reineri, *ChemPhysChem* **2021**, *22*, 1042–1048.
- [68] Y. Ding, S. Korchak, S. Mamone, A. P. Jagtap, G. Stevanato, S. Sternkopf, D. Moll, H. Schroeder, S. Becker, A. Fischer, E. Gerhardt, T. F. Outeiro, F. Opazo, C. Griesinger, S. Glöggler, *Chemistry–Methods* **2022**, *2*, e202200023.
- [69] A. Brahms, A. N. Pravdivtsev, T. Stamp, F. Ellermann, F. D. Sönnichsen, J.-B. Hövener, R. Herges, *Chem. – Eur. J.* **2022**, *28*, e202201210.
- [70] M. T. Huynh, Z. Kovacs, *Anal. Sens.* **2024**, e202400044.
- [71] O. G. Salnikov, N. V. Chukanov, L. M. Kovtunova, V. I. Bukhtiyarov, K. V. Kovtunov, R. V. Shchepin, I. V. Koptyug, E. Y. Chekmenev, *ChemPhysChem* **2021**, 1389–1396.

- [72] O. G. Salnikov, N. V. Chukanov, R. V. Shchepin, I. V. Manzanera Esteve, K. V. Kovtunov, I. V. Koptuyug, E. Y. Chekmenev, *J. Phys. Chem. C* **2019**, *123*, 12827–12840.
- [73] A. N. Pravdivtsev, A. Brahms, S. Kienitz, F. D. Sönnichsen, J.-B. Hövener, R. Herges, *ChemPhysChem* **2021**, *22*, 370–377.
- [74] M. Itoda, Y. Naganawa, M. Ito, H. Nonaka, S. Sando, *RSC Adv.* **2019**, *9*, 18183–18190.
- [75] O. Bondar, E. Cavallari, C. Carrera, S. Aime, F. Reineri, *Catal. Today* **2022**, *397–399*, 94–102.
- [76] J. Bargon, J. Kandels, P. Kating, *J. Chem. Phys.* **1993**, *98*, 6150–6153.
- [77] J. Natterer, O. Schedletzky, J. Barkemeyer, J. Bargon, S. J. Glaser, *J. Magn. Reson.* **1998**, *133*, 92–97.
- [78] A. N. Pravdivtsev, A. Brahms, F. Ellermann, T. Stamp, R. Herges, J.-B. Hövener, *Sci. Rep.* **2022**, *12*, 19361.
- [79] O. Mohiuddin, H. de Maissin, A. N. Pravdivtsev, A. Brahms, M. Herzog, L. Schröder, E. Y. Chekmenev, R. Herges, J.-B. Hövener, M. Zaitsev, D. von Elverfeldt, A. B. Schmidt, *Commun. Chem.* **2024**, *7*, 240.
- [80] S. Korchak, S. Mamone, S. Glöggler, *ChemistryOpen* **2018**, *7*, 672–676.
- [81] F. Ellermann, A. Sirbu, A. Brahms, C. Assaf, R. Herges, J.-B. Hövener, A. N. Pravdivtsev, *Nat. Commun.* **2023**, *14*, 4774.
- [82] S. Berner, A. B. Schmidt, M. Zimmermann, A. N. Pravdivtsev, S. Glöggler, J. Hennig, D. von Elverfeldt, J.-B. Hövener, *ChemistryOpen* **2019**, *8*, 728–736.
- [83] D. A. Markelov, V. P. Kozinenko, S. Knecht, A. S. Kiryutin, A. V. Yurkovskaya, K. L. Ivanov, *Phys. Chem. Chem. Phys.* **2021**, *23*, 20936–20944.
- [84] P. Kating, A. Wandelt, R. Selke, J. Bargon, *J. Phys. Chem.* **1993**, *97*, 13313–13317.
- [85] E. V. Pokochueva, D. B. Burueva, O. G. Salnikov, I. V. Koptuyug, *ChemPhysChem* **2024**, *25*, e202400209.
- [86] E. A. Nasibulov, A. N. Pravdivtsev, A. V. Yurkovskaya, N. N. Lukzen, H.-M. Vieth, K. L. Ivanov, *Z. Phys. Chem.* **2013**, *227*, 929–953.
- [87] M. Goldman, H. Jóhannesson, *Comptes Rendus Phys.* **2005**, *6*, 575–581.
- [88] J. Natterer, J. Bargon, *Prog. Nucl. Magn. Reson. Spectrosc.* **1997**, *31*, 293–315.
- [89] N. J. Stewart, H. Kumeta, M. Tomohiro, T. Hashimoto, N. Hatae, S. Matsumoto, *J. Magn. Reson.* **2018**, *296*, 85–92.
- [90] A. N. Pravdivtsev, F. Ellermann, J. B. Hövener, *Phys. Chem. Chem. Phys.* **2021**, *23*, 14146–14150.
- [91] A. Svyatova, V. P. Kozinenko, N. V. Chukanov, D. B. Burueva, E. Y. Chekmenev, Y.-W. Chen, D. W. Hwang, K. V. Kovtunov, I. V. Koptuyug, *Sci. Rep.* **2021**, *11*, 5646.
- [92] L. Dagys, A. P. Jagtap, S. Korchak, S. Mamone, P. Saul, M. H. Levitt, S. Glöggler, *Analyst* **2021**, *146*, 1772–1778.
- [93] A. N. Pravdivtsev, D. A. Barskiy, J.-B. Hövener, I. V. Koptuyug, *Symmetry* **2022**, *14*, 530.
- [94] G. A. Morris, R. Freeman, *J. Am. Chem. Soc.* **1979**, *101*, 760–762.
- [95] R. A. Green, R. W. Adams, S. B. Duckett, R. E. Mewis, D. C. Williamson, G. G. R. Green, *Prog. Nucl. Magn. Reson. Spectrosc.* **2012**, *67*, 1–48.
- [96] M. Haake, J. Natterer, J. Bargon, *J. Am. Chem. Soc.* **1996**, *118*, 8688–8691.
- [97] A. N. Pravdivtsev, J.-B. Hövener, A. B. Schmidt, *ChemPhysChem* **2022**, *23*, e202100721.
- [98] G. Stevanato, *J. Magn. Reson.* **2017**, *274*, 148–162.
- [99] S. Berner, A. B. Schmidt, F. Ellermann, S. Korchak, E. Y. Chekmenev, S. Glöggler, D. von Elverfeldt, J. Hennig, J.-B. Hövener, *Phys. Chem. Chem. Phys.* **2021**, *23*, 2320–2330.
- [100] J. McCormick, S. Korchak, S. Mamone, Y. N. Ertas, Z. Liu, L. Verlinsky, S. Wagner, S. Glöggler, L.-S. Bouchard, *Angew. Chem. Int. Ed.* **2018**, *57*, 10692–10696.
- [101] S. S. Roy, G. Stevanato, P. J. Rayner, S. B. Duckett, *J. Magn. Reson.* **2017**, *285*, 55–60.
- [102] C. D. Assaf, X. Gui, A. A. Auer, S. B. Duckett, J.-B. Hövener, A. N. Pravdivtsev, *J. Phys. Chem. Lett.* **2024**, *15*, 1195–1203.
- [103] A. N. Pravdivtsev, A. V. Yurkovskaya, H. Zimmermann, H.-M. Vieth, K. L. Ivanov, *Chem. Phys. Lett.* **2016**, *661*, 77–82.
- [104] C. D. Assaf, X. Gui, O. G. Salnikov, A. Brahms, N. V. Chukanov, I. V. Skovpin, E. Y. Chekmenev, R. Herges, S. B. Duckett, I. V. Koptuyug, K. Buckenmaier, R. Körber, M. Plaumann, A. A. Auer, J.-B. Hövener, A. N. Pravdivtsev, *Commun. Chem.* **2024**, *7*, 286.
- [105] K. D. Atkinson, M. J. Cowley, S. B. Duckett, P. I. P. Elliott, G. G. R. Green, J. Lopez-Serrano, I. G. Khazal, A. C. Whitwood, *Inorg. Chem.* **2009**, *48*, 663–670.
- [106] A. B. Schmidt, A. Brahms, F. Ellermann, S. Knecht, S. Berner, J. Hennig, D. Von Elverfeldt, R. Herges, J.-B. Hövener, A. N. Pravdivtsev, *Phys. Chem. Chem. Phys.* **2021**, *23*, 26645–26652.
- [107] G. Stevanato, Y. Ding, S. Mamone, A. P. Jagtap, S. Korchak, S. Glöggler, *J. Am. Chem. Soc.* **2023**, *145*, 5864–5871.
- [108] A. N. Pravdivtsev, A. V. Yurkovskaya, N. N. Lukzen, K. L. Ivanov, H.-M. Vieth, *J. Phys. Chem. Lett.* **2014**, *5*, 3421–3426.
- [109] A. Marshall, A. Salhov, M. Gierse, C. Müller, M. Keim, S. Lucas, A. Parker, J. Scheuer, C. Vassiliou, P. Neumann, F. Jelezko, A. Retzker, J. W. Blanchard, I. Schwartz, S. Knecht, *J. Phys. Chem. Lett.* **2023**, *14*, 2125–2132.
- [110] S. Kadlec, K. Emami, M. Ishii, R. Rizi, *J. Magn. Reson.* **2010**, *205*, 9–13.
- [111] M. Goldman, H. Jóhannesson, O. Axelsson, M. Karlsson, *Magn. Reson. Imaging* **2005**, *23*, 153–157.
- [112] K. L. Ivanov, A. N. Pravdivtsev, A. V. Yurkovskaya, H.-M. Vieth, R. Kaptein, *Prog. Nucl. Magn. Reson. Spectrosc.* **2014**, *81*, 1–36.
- [113] J. Eills, J. W. Blanchard, T. Wu, C. Bengs, J. Hollenbach, D. Budker, M. H. Levitt, *J. Chem. Phys.* **2019**, *150*, 174202.
- [114] B. A. Rodin, K. L. Ivanov, *Magn. Reson.* **2020**, *1*, 347–365.

- [115] E. Cavallari, C. Carrera, S. Aime, F. Reineri, *ChemPhysChem* **2019**, *20*, 318–325.
- [116] E. Cavallari, C. Carrera, G. Di Matteo, O. Bondar, S. Aime, F. Reineri, *Front. Oncol.* **2020**, *10*, 497.
- [117] B. Joalland, A. B. Schmidt, M. S. H. Kabir, N. V. Chukanov, K. V. Kovtunov, I. V. Koptug, J. Hennig, J.-B. Hövener, E. Y. Chekmenev, *Anal. Chem.* **2020**, *92*, 1340–1345.
- [118] B. Joalland, E. Y. Chekmenev, *J. Phys. Chem. Lett.* **2022**, *13*, 1925–1930.
- [119] V. P. Kozinenko, A. S. Kiryutin, A. V. Yurkovskaya, *J. Chem. Phys.* **2022**, *157*, 174201.
- [120] S. Bär, T. Lange, D. Leibfritz, J. Hennig, D. von Elverfeldt, J.-B. Hövener, *J. Magn. Reson.* **2012**, *225*, 25–35.
- [121] K. Them, F. Ellermann, A. N. Pravdivtsev, O. G. Salnikov, I. V. Skovpin, I. V. Koptug, R. Herges, J.-B. Hövener, *J. Am. Chem. Soc.* **2021**, *143*, 13694–13700.
- [122] K. Them, J. Kuhn, A. N. Pravdivtsev, J.-B. Hövener, *Commun. Chem.* **2024**, *7*, 172.
- [123] B. J. Tickner, V. V. Zhivonitko, *Chem. Sci.* **2022**, *13*, 4670–4696.
- [124] A. B. Schmidt, C. R. Bowers, K. Buckenmaier, E. Y. Chekmenev, H. de Maissin, J. Eills, F. Ellermann, S. Glöggler, J. W. Gordon, S. Knecht, I. V. Koptug, J. Kuhn, A. N. Pravdivtsev, F. Reineri, T. Theis, K. Them, J.-B. Hövener, *Anal. Chem.* **2022**, *94*, 479–502.
- [125] H. Desvaux, *Prog. Nucl. Magn. Reson. Spectrosc.* **2013**, *70*, 50–71.
- [126] M. H. Levitt, *Concepts Magn. Reson.* **1996**, *8*, 77–103.
- [127] S. Korchak, M. Emondts, S. Mamone, B. Blümich, S. Glöggler, *Phys. Chem. Chem. Phys.* **2019**, *21*, 22849–22856.
- [128] M. Siefert, S. Lehmkuhl, A. Liebisch, B. Blümich, S. Appelt, *Nat. Phys.* **2017**, *13*, 568–572.
- [129] S. Appelt, A. Kentner, S. Lehmkuhl, B. Blümich, *Prog. Nucl. Magn. Reson. Spectrosc.* **2019**, *114–115*, 1–32.
- [130] A. N. Pravdivtsev, F. D. Sönnichsen, J.-B. Hövener, *ChemPhysChem* **2020**, *21*, 667–672.
- [131] B. Joalland, N. M. Ariyasingha, S. Lehmkuhl, T. Theis, S. Appelt, E. Y. Chekmenev, *Angew. Chem. Int. Ed.* **2020**, *59*, 8654–8660.
- [132] S. Korchak, L. Kaltschnee, R. Dervisoglu, L. Andreas, C. Griesinger, S. Glöggler, *Angew. Chem. Int. Ed.* **2021**, *60*, 20984–20990.
- [133] O. G. Salnikov, I. A. Trofimov, A. N. Pravdivtsev, K. Them, J.-B. Hövener, E. Y. Chekmenev, I. V. Koptug, *Anal. Chem.* **2022**, *94*, 15010–15017.
- [134] T. R. Eichhorn, A. J. Parker, F. Josten, C. Müller, J. Scheuer, J. M. Steiner, M. Gierse, J. Handwerker, M. Keim, S. Lucas, M. U. Qureshi, A. Marshall, A. Salhov, Y. Quan, J. Binder, K. D. Jahnke, P. Neumann, S. Knecht, J. W. Blanchard, M. B. Plenio, F. Jelezko, L. Emsley, C. C. Vassiliou, P. Hautle, I. Schwartz, *J. Am. Chem. Soc.* **2022**, *144*, 2511–2519.
- [135] B. Joalland, T. Theis, S. Appelt, E. Y. Chekmenev, *Angew. Chem. Int. Ed.* **2021**, *60*, 26298–26302.
- [136] A. B. Schmidt, I. Adelabu, C. Nelson, S. Nantogma, V. G. Kiselev, M. Zaitsev, A. Abdurraheem, H. de Maissin, M. S. Rosen, S. Lehmkuhl, S. Appelt, T. Theis, E. Y. Chekmenev, *J. Am. Chem. Soc.* **2023**, *145*, 11121–11129.
- [137] S. Nantogma, H. de Maissin, I. Adelabu, A. Abdurraheem, C. Nelson, N. V. Chukanov, O. G. Salnikov, I. V. Koptug, S. Lehmkuhl, A. B. Schmidt, S. Appelt, T. Theis, E. Y. Chekmenev, *ACS Sens.* **2024**, *9*, 770–780.
- [138] L. Dagys, M. C. Korzeczek, A. J. Parker, J. Eills, J. W. Blanchard, C. Bengs, M. H. Levitt, S. Knecht, I. Schwartz, M. B. Plenio, *Sci. Adv.* **2024**, *10*, eado0373.
- [139] M. Lee, W. I. Goldberg, *Phys. Rev.* **1965**, *140*, A1261–A1271.
- [140] W. I. Goldberg, M. Lee, *Phys. Rev. Lett.* **1963**, *11*, 255–258.
- [141] T. Trantzschele, J. Bernarding, M. Plaumann, D. Lego, T. Gutmann, T. Ratajczyk, S. Dillenberger, G. Buntkowsky, J. Bargon, U. Bommerich, *Phys. Chem. Chem. Phys.* **2012**, *14*, 5601–5604.
- [142] F. Reineri, A. Viale, S. Ellena, T. Boi, V. Daniele, R. Gobetto, S. Aime, *Angew. Chem. Int. Ed.* **2011**, *50*, 7350–7353.
- [143] E. Cavallari, C. Carrera, S. Aime, F. Reineri, *J. Magn. Reson.* **2018**, *289*, 12–17.
- [144] J. Halpern, *Science* **1982**, *217*, 401–407.
- [145] A. Preetz, C. Fischer, C. Kohrt, H.-J. Drexler, W. Baumann, D. Heller, *Organometallics* **2011**, *30*, 5155–5159.
- [146] K. V. Kovtunov, D. A. Barskiy, R. V. Shchepin, O. G. Salnikov, I. P. Prosvirin, A. V. Bukhtiyarov, L. M. Kovtunova, V. I. Bukhtiyarov, I. V. Koptug, E. Y. Chekmenev, *Chem. – Eur. J.* **2016**, *22*, 16446–16449.
- [147] J. McCormick, A. M. Grunfeld, Y. N. Ertas, A. N. Biswas, K. L. Marsh, S. Wagner, S. Glöggler, L.-S. Bouchard, *Anal. Chem.* **2017**, *89*, 7190–7194.
- [148] L. Kaltschnee, A. P. Jagtap, J. McCormick, S. Wagner, L.-S. Bouchard, M. Utz, C. Griesinger, S. Glöggler, *Chem. – Eur. J.* **2019**, *25*, 11031–11035.
- [149] O. Warburg, *Science* **1956**, *123*, 309–314.
- [150] M. V. Liberti, J. W. Locasale, *Trends Biochem. Sci.* **2016**, *41*, 211–218.
- [151] R. L. Hesketh, K. M. Brindle, *Curr. Opin. Chem. Biol.* **2018**, *45*, 187–194.
- [152] M. D. Santi, T. L. K. Hune, G. G. Rodriguez, L. M. Fries, R. Mei, S. Sternkopf, J. Elsaßer, S. Glöggler, *Analyst* **2024**, *149*, 5022–5033.
- [153] Y. Ding, G. Stevanato, F. von Bonin, D. Kube, S. Glöggler, *Chem. Sci.* **2023**, *14*, 7642–7647.
- [154] G. Sapir, D. J. Steinberg, R. I. Aqeilan, R. Katz-Brull, *Pharmaceuticals* **2021**, *14*, 878.
- [155] T. B. W. Mathiassen, A. E. Høgh, M. Karlsson, S. Katsikis, K. Wang, M. Pennestri, J. H. Ardenkjær-Larsen, P. R. Jensen, *J. Magn. Reson. Open* **2023**, *16–17*, 100131.
- [156] L. M. Fries, T. L. K. Hune, S. Sternkopf, S. Mamone, K. L. Schneider, R. Schulz-Heddergott, D.

- Becker, S. Glögler, *Chem. – Eur. J.* **2024**, *30*, e202400187.
- [157] T. L. K. Hune, S. Mamone, A. B. Schmidt, I. Mahú, N. D'Apolito, D. Wiedermann, J. Brüning, S. Glögler, *Appl. Magn. Reson.* **2023**, *54*, 1283–1295.
- [158] V. V. Zlobina, A. S. Kiryutin, I. A. Nikovskiy, O. I. Artyushin, V. P. Kozinenko, A. S. Peregudov, A. V. Yurkovskaya, V. V. Novikov, *Int. J. Mol. Sci.* **2023**, *24*, 557.